

Hippocampal CA2 sharp-wave ripples reactivate and promote social memory

<https://doi.org/10.1038/s41586-020-2758-y>

Azahara Oliva¹✉, Antonio Fernández-Ruiz², Félix Leroy¹ & Steven A. Siegelbaum^{1,3}✉

Received: 21 November 2019

Accepted: 25 June 2020

Published online: 23 September 2020

 Check for updates

The consolidation of spatial memory depends on the reactivation ('replay') of hippocampal place cells that were active during recent behaviour. Such reactivation is observed during sharp-wave ripples (SWRs)—synchronous oscillatory electrical events that occur during non-rapid-eye-movement (non-REM) sleep^{1–8} and whose disruption impairs spatial memory^{3,5,6,8}. Although the hippocampus also encodes a wide range of non-spatial forms of declarative memory, it is not yet known whether SWRs are necessary for such memories. Moreover, although SWRs can arise from either the CA3 or the CA2 region of the hippocampus^{7,9}, the relative importance of SWRs from these regions for memory consolidation is unknown. Here we examine the role of SWRs during the consolidation of social memory—the ability of an animal to recognize and remember a member of the same species—focusing on CA2 because of its essential role in social memory^{10–12}. We find that ensembles of CA2 pyramidal neurons that are active during social exploration of previously unknown conspecifics are reactivated during SWRs. Notably, disruption or enhancement of CA2 SWRs suppresses or prolongs social memory, respectively. Thus, SWR-mediated reactivation of hippocampal firing related to recent experience appears to be a general mechanism for binding spatial, temporal and sensory information into high-order memory representations, including social memory.

To study the role of SWRs in social memory, we used a social-recognition task that assesses social-memory formation in mice without interference from other social behaviours. In this task, a subject mouse is habituated to a square arena with two empty wire cups in opposite corners. After habituation, a previously unknown 'stimulus' mouse is placed in each of the cups (mice S₁ and S₂). In trial 1, the subject mouse is allowed to explore the arena and stimulus animals for five minutes; this phase is followed by a second five-minute trial with the positions of the same stimulus mice rotated 180° relative to trial 1 (Fig. 1a and Extended Data Fig. 1a, b). A one-hour sleep session precedes (pre-sleep) and follows (post-sleep) the two learning trials. After the post-sleep period, one of the stimulus mice (chosen at random) is exchanged for a third novel mouse (N) and a memory-recall trial is performed.

We found that animals interacted for equal times with mice S₁ and S₂ in the two learning trials, but showed a significant preference, in terms of increased interaction time, for the novel versus the now-familiar stimulus mouse in the recall trial; this preference was quantified using a discrimination index (Fig. 1b and Methods). No other behavioural differences were noted between learning and recall trials (Extended Data Fig. 1c, d). The preference for the novel mouse demonstrated the successful encoding and consolidation of social memory of the stimulus mice.

CA2 cells remap to a social stimulus

To explore how the different regions of the hippocampus encode social and spatial information during this task, we implanted high-density

silicon probes in the dorsal hippocampus (Fig. 1c, Extended Data Fig. 2 and Supplementary Table 1) and analysed the spatial firing patterns of 140 CA1 (8 mice), 473 CA2 (13 mice), and 64 CA3 (5 mice) pyramidal neurons. We verified the location of the probes using post hoc histology (Fig. 1c), including immunocytochemical staining for CA2-specific markers in the CA2-selective Amigo2–Cre mouse line¹⁰. We observed two main effects on the spatial firing properties of pyramidal neurons (place fields) when we switched the positions and identities of the stimulus mice in this task (see Methods). Some cells, which we term 'social-invariant cells', displayed stable place fields relative to the arena across trials (Fig. 1d, upper panels, and Extended Data Fig. 3). By contrast, other cells, termed 'social-remapping cells', showed place fields that remapped between the trials in a way that maintained the firing field's position relative to the location of a particular stimulus mouse (Fig. 1d, bottom panels, and Extended Data Fig. 3). We quantified this phenomenon by comparing the spatial correlation of firing maps between the two learning trials with the correlation obtained by rotating the map in trial 2 by 180° to match the position of the same stimulus mice in trial 1 (Extended Data Fig. 4). We performed a similar comparison between place fields around the stimulus mouse in the recall trial with place fields around that same stimulus mouse in the relevant learning trial (the one in which it was in the opposite corner to the recall trial).

Unsupervised clustering of the unrotated versus rotated correlation values for all neurons revealed several clusters. One subpopulation of neurons (30% of the cells) had maximal unrotated and minimal

¹Department of Neuroscience, The Kavli Institute for Brain Science, Mortimer B. Zuckerman Mind Brain Behavior Institute, Columbia University, New York, NY, USA. ²New York University Neuroscience Institute, New York University, New York, NY, USA. ³Department of Pharmacology, Vagelos College of Physicians and Surgeons, Columbia University, New York, NY, USA.
✉e-mail: azaharaglez@gmail.com; sas@columbia.edu

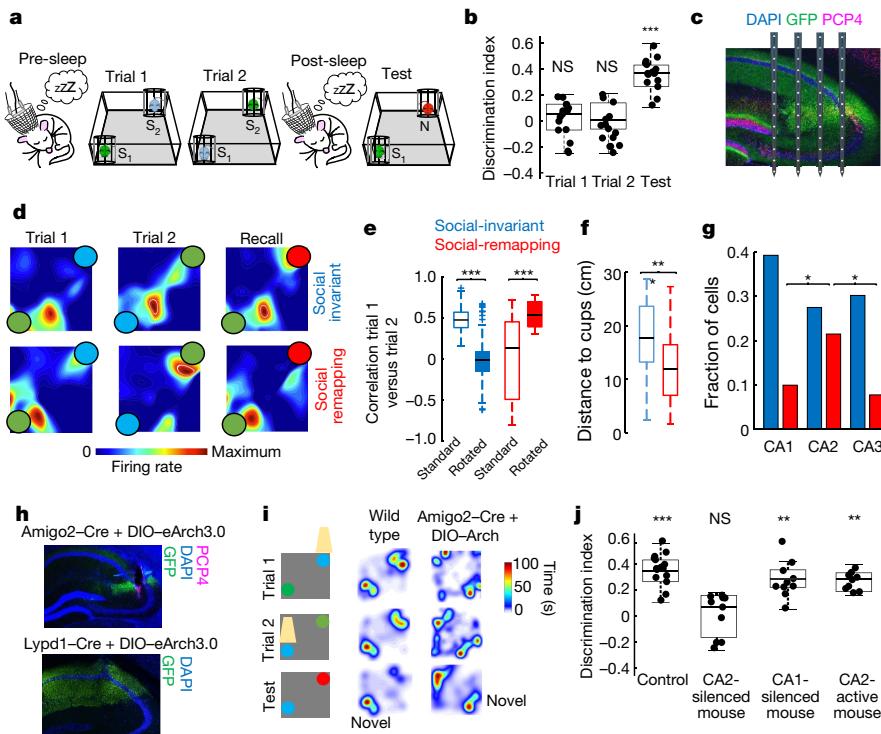


Fig. 1 | Encoding of conspecifics by activity of CA2 pyramidal cells. **a**, Schema of the task (coloured mice in wire cups have been modified from the Clipart Library, number 1335742). **b**, Social memory in wild-type mice during recall trial ('test'), quantified by discrimination index (see Methods; $n=13$). *** $P<0.001$, Wilcoxon sign-rank test. NS, not significant. In box plots, the central lines indicate medians; the bottom and top edges indicate the 25th and 75th percentiles respectively; whiskers extend to the most extreme data points (excluding outliers); and dots indicate individual data points. **c**, Histological verification of probe location in CA1, CA2 and CA3 regions. Blue, DNA staining with 4',6-diamidino2-phenylindole (DAPI); green, Cre-dependent viral expression of green fluorescent protein (GFP) in Amigo2-Cre mouse; pink, PCP4 immunolabelling of CA2 pyramidal cells with Purkinje cell protein 4 (PCP4). **d**, Example firing maps from social-invariant and social-remapping CA2 place cells. **e**, Pearson's correlation values for unrotated and rotated place fields in trials 1 and 2 for social-invariant cells (blue; $n=203$ from 13 mice; $P<10^{-54}$, sign-rank test) and social-remapping cells (red; $n=120$ from 13 mice; $P<10^{-10}$, rank-sum test). **f**, Social-remapping cells had place fields closer to the location of the stimulus mice than social-invariant cells ($P<10^{-10}$, rank-sum test). * $P<0.01$; ** $P<0.001$. **g**, Proportion of social-invariant and social-remapping cells per region. Social-remapping cells were more abundant in CA2 than CA1 ($P<0.05$, Fisher's test) or CA3 ($P<0.05$). CA1: 55 social-invariant and 14 social-remapping cells; CA2: 131 social-invariant and 101 social-remapping cells; CA3: 17 social-invariant and 5 social-remapping cells. **h**, Protocol for examining the role of CA2 and CA1 in social memory using eArch3.0-GFP expression (green) in CA2

pyramidal cells of an Amigo2-Cre mouse (top) or in CA1 cells of an Lypd1-Cre mouse (bottom). **i**, Yellow light was applied to activate eArch3.0 and to silence CA1 or CA2 only during periods when a subject mouse entered an interaction zone surrounding one of the two stimulus mice (blue mouse); light was applied during both learning trials 1 and 2. CA2 remained active when the subject mouse interacted with the other stimulus mouse (green mouse).

j, Social-memory recall was present in a control group, whose discrimination index was significantly greater than 0 ($P<0.001$, *t*-test). The control group consisted of Cre⁺ ($n=7$) and Cre⁻ ($n=6$) animals injected with virus without light stimulation; no difference was found in the discrimination indices between the two control subgroups ($P>0.05$, rank-sum test). Applying light to Cre⁺ mice expressing eArch3.0 in CA2 as the subject mouse interacted with a given stimulus mouse abolished memory of that mouse in the recall trial ('CA2-silenced mouse' group; discrimination index not significantly greater than 0; $n=10$ mice; $P>0.05$, *t*-test); memory was intact for the stimulus mouse around which CA2 remained active ('CA2-active mouse' group; discrimination index significantly greater than 0; $n=11$ mice, $P<0.001$, *t*-test); CA1 silencing during interactions with a given stimulus mouse had no effect on social memory for that mouse (CA1-silenced mouse group; discrimination index significantly greater than 0; $n=10$; $P<0.001$, *t*-test). Multiple comparison test and Tukey's post hoc tests between the groups showed that the discrimination index for the CA2-silenced mouse group was significantly less than that of the control group ($P<0.001$), CA1-silenced mouse group ($P<0.001$) and CA2-active mouse group ($P<0.01$).

rotated correlation values, which we define as social-invariant place cells. A second subpopulation (18% of the cells) had maximal rotated and minimal unrotated correlation values when compared across the two learning trials (Fig. 1e and Extended Data Fig. 4a–d) or across the recall trial with the relevant learning trial (Extended Data Fig. 4e); we define these as social-remapping place cells.

Place fields of social-remapping cells lay closer to the cups containing stimulus mice than did place fields of social-invariant cells (Fig. 1f and Extended Data Fig. 4f); otherwise, the two cell types displayed similar properties (Extended Data Figs. 4g, h, 5a–g), with similar immobility modulation^{9,13}, head-direction tuning¹⁴ and preferred theta phase⁹ (Extended Data Fig. 5h–m). Social-remapping cells were significantly more abundant in the CA2 region than in CA1 or CA3 (Fig. 1g), consistent with the selective role of dorsal CA2 in social memory^{10–12}.

Dorsal CA2 is needed for social memory

To explore the relevance of the social-coding properties of CA1 and CA2 pyramidal neurons, we investigated their contributions to the performance of the social-memory task. We expressed the inhibitory opsin archaerhodopsin 3.0 using Cre-dependent adeno-associated viral injections (AAV2/5EF1a.DIO.eArch3.0-eYFP) into dorsal CA2 or dorsal CA1 of the CA2-selective Amigo2-Cre mouse line¹⁰ or the CA1-selective Lypd1-Cre line¹⁵, respectively. The animals were implanted with bilateral optic fibres over CA2 or CA1 (Fig. 1h). We selectively silenced CA2 or CA1 pyramidal cells by applying continuous yellow light during periods when a subject mouse entered an interaction zone around either S₁ or S₂ (the mouse being chosen at random for each experiment) during both learning trials (Fig. 1i). We found that silencing CA2 during the time

that a subject interacted with a given stimulus mouse disrupted social memory of that stimulus mouse in the recall trial, but had no effect on memory in the recall trial for the stimulus mouse around which CA2 was allowed to remain active; silencing CA1 when a subject mouse interacted with a given stimulus mouse failed to disrupt memory for that mouse (Fig. 1j; $F(3,41) = 13.42$, one-way ANOVA followed by Tukey's post hoc test compared to control group; $P < 0.003$ for stimulus mouse around which CA2 was silenced; $P > 0.05$ for stimulus mouse with CA2 active; $P > 0.05$ for stimulus mouse with CA1 silenced). These results extend previous reports on the importance of dorsal CA2^{10–12} for social-memory formation by showing the specific requirement for CA2 activity during active exploration of a given animal.

To determine whether CA2 plays a general role in novelty encoding, we used a behavioural paradigm analogous to the social-memory task, in which a mouse explored two previously unknown objects in learning trial 1, whose positions were then exchanged in learning trial 2. This is known to cause remapping of place fields in a fraction of CA1 neurons¹⁶. After a one-hour interval, we carried out a memory-recall test by measuring relative exploration times for one object from the learning trials versus a third novel object (Extended Data Fig. 6). As expected, animals preferred to explore the novel object during the recall trial (Extended Data Fig. 6b), similar to their preference for a novel animal. To examine the relative importance of dorsal CA1 versus dorsal CA2 for performance of this task, we expressed eArch3.0 in each region selectively, as above. In contrast with the finding that dorsal CA2 but not dorsal CA1 was essential for social memory, we observed a significant impairment in novel object recognition memory when we optogenetically silenced CA1 but not when we silenced CA2 (Extended Data Fig. 6b, $F(2,28) = 5.01$, $P = 0.014$, one-way ANOVA; $P < 0.01$ for wild-type versus CA1 group, $P > 0.05$ for wild-type versus CA2 and $P > 0.05$ for CA1 versus CA2 group, Tukey's post hoc test). This confirms previous results that dorsal CA2 is not required for novel object memory¹⁰.

Next we examined whether CA2 place fields remapped when we swapped the position of the novel objects. We calculated the rotated versus unrotated correlations of the firing maps upon exchange of object location during the learning trials to classify place cells as 'object-remapping' or 'object-invariant', akin to our classification of social-remapping cells. We found that all CA regions contained both object-remapping and object-invariant place cells (Extended Data Fig. 6c, d), just as they all contained social-remapping and social-invariant place cells. However, whereas CA2 contained a significantly higher fraction of social-remapping place cells than CA1 or CA3, CA2 had a significantly lower proportion of object-remapping place cells than CA1 and CA3 (Extended Data Fig. 6e–g). Thus, although the three CA regions each contain populations of cells whose firing is selectively tuned to objects, conspecifics and/or spatial location, CA2 is enriched in social representations compared with its hippocampal neighbours, consistent with previous reports^{10,11}.

Social memory requires CA2 SWRs

Given the importance of SWRs in spatial memory consolidation^{1,3,5,7} and of CA2 in generating a substantial fraction of SWRs⁹, we next explored whether SWRs provide a neural substrate of social-memory consolidation in the social recognition task. We observed a significant increase in the rate of SWRs during the post-sleep session compared with the pre-sleep session (Fig. 2a), similar to the increase in SWRs seen in rodents following spatial learning¹⁷.

To test whether SWRs are necessary for social-memory consolidation, we performed closed-loop optogenetic disruption of SWRs during the consolidation stage (post-sleep) of the task in Amigo2-Cre mice expressing ChR2 in CA2 using injection of a Cre-dependent viral vector (AAV2/5 EF1a.DIO.hChR2.eYFP) (Fig. 2b). Strong photostimulation of CA2 pyramidal neurons with a brief intense light pulse upon SWR detection⁸ resulted in the premature termination of SWRs, with a period of

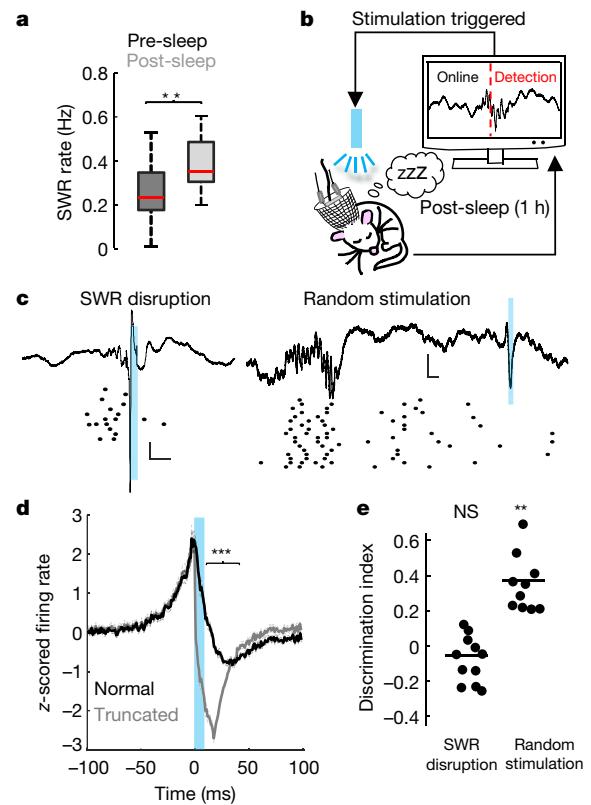


Fig. 2 | Effect of SWR disruption on social-memory consolidation. **a**, The SWR rate in CA2 increased during the post-sleep session following social learning trials by comparison with pre-sleep sessions ($n = 17$ mice; $P < 0.01$, rank-sum test). **b**, Experimental approach for disrupting SWRs during sleep consolidation periods. **c**, SWRs were disrupted by strong activation of ChR2 expressed in CA2 pyramidal neurons with a 10-ms, high-intensity, blue-light pulse upon real-time detection of ripples in CA2. Examples are shown of SWR disruption (left plot) and a control experiment in which ChR2 was activated at a random delay after a SWR (right plot). Traces show local field potentials (LFPs) from the CA2 pyramidal layer (top) and raster plot firing of CA2 units (bottom). Vertical scale, 0.2 mV; horizontal scale, 20 ms. **d**, The average firing rate of pyramidal cells decreased during disrupted (truncated, grey) compared with normal (black) SWRs ($P < 10^{-4}$, rank-sum test; $n = 7$). **e**, Social-memory recall was impaired following CA2 ripple disruption ($P > 0.05$, $n = 11$ sessions in $n = 7$ mice) but preserved following random delayed stimulation ($P = 0.002$, $n = 10$ sessions in $n = 7$ mice).

post-excitation inhibition of CA2 firing (Fig. 2c,d and Extended Data Fig. 7c,d). In control sessions, we delivered the same light pulse after a random delay upon SWR detection (Fig. 2c). We found that disrupting SWRs during the post-sleep session impaired social-memory recall, whereas random stimulation had no effect (Fig. 2e). As an alternative approach, we silenced CA2 neurons with photoactivation of eArch3.0 for 30 seconds once every 2 minutes during the post-sleep period (Extended Data Fig. 7e,f); this reduced the number of SWRs and significantly impaired social-memory recall (Extended Data Fig. 7g,h). Together, these results show that CA2 SWRs are necessary for social-memory consolidation. Of note, in contrast with the inhibitory effects on SWRs of brief periods of CA2 silencing, longer periods of CA2 silencing can increase the occurrence of SWRs¹⁸, probably as a result of disinhibition of CA3 (ref. ¹⁹).

CA2 SWRs replay social memory

SWRs during sleep following spatial learning have been shown to reactivate place cells that fired during spatial exploration, serving to replay

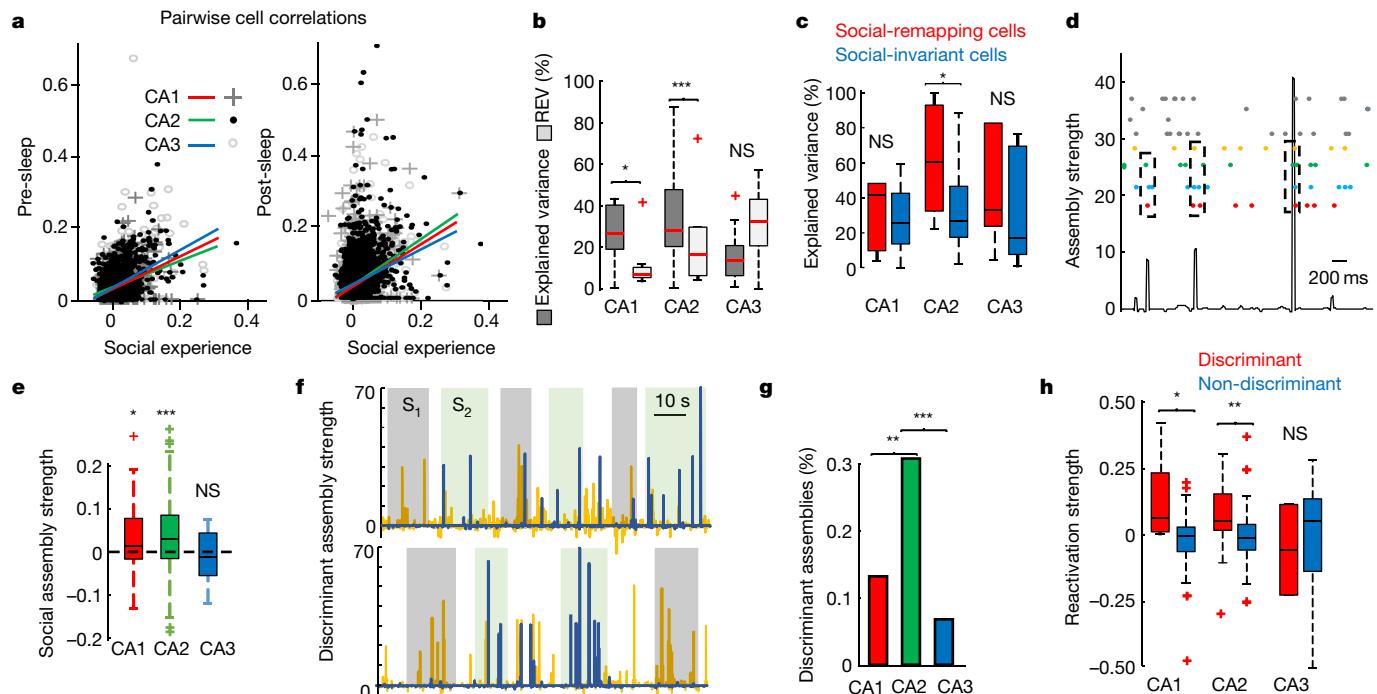


Fig. 3 | Reactivation during sleep of cell ensembles that were active during prior social learning. **a**, Pearson's pairwise correlation coefficients for all pairs of CA1, CA2 and CA3 neurons measured during pre-sleep (left) or post-sleep (right) sessions versus correlations measured during social learning trials. Lines show least-squares linear fits for pre-sleep ($R=0.165, 0.189, 0.213$ and $P=0.031, 0.029, 0.035$ for CA1, CA2, CA3, respectively) and post-sleep ($R=0.231, 0.223, 0.211$ and $P=0.034, 0.035, 0.035$ for CA1, CA2, CA3, respectively) versus social sessions. Note the greater correlations during the post-sleep versus social-session plot compared with the pre-sleep versus social-session plot ($P<0.0001$ for CA1, CA2 and CA3 groups, Wilcoxon sign-rank test). **b**, Explained variance (see Methods) was significantly higher than chance, measured by reverse explained variance (REV), for CA2 ($P=0.0028, n=13$ sessions) and CA1 ($P=0.03, n=13$ sessions) cells but not CA3 cells ($P>0.05, n=7$ sessions). Plus symbols indicate outliers (approximately over 2.7 standard deviations; see Methods). **c**, Explained variance for social-remapping cells versus social-invariant cells in each area. Explained variance was significantly greater for social-remapping versus social-invariant cells in CA2 ($P<0.05$, sign-rank test) but not CA1 or CA3 ($P>0.05$, sign-rank

test). **d**, Example of assembly detection. Each line of the raster plot shows the firing of one CA2 unit; units in the example assembly, which contained four cells, are coloured. Bottom trace, activation strength (see Methods) for example assembly. **e**, Social-related assembly strength, (assembly strength inside minus strength outside social interaction zones)/(sum of strengths), was significantly greater than 0 for CA1 ($P<10^{-6}$, sign-rank test) and CA2 ($P<10^{-19}$) cells but not CA3 cells ($P>0.05$). Plus symbols indicate outliers. **f**, Activation of social-discriminант assemblies (those activated more strongly around one mouse versus the other; see Methods). Shown are examples of one CA2 assembly (yellow line) that is more strongly activated around mouse S₁ than around S₂ (grey and green bars, respectively) and a second assembly (blue line) that is more active around mouse S₂. **g**, Fraction of assemblies in each region that were social-discriminант ($P<0.0034$ and 10^{-4} for CA2 versus CA1 and CA3, respectively, Fisher's test). **h**, Assembly-reactivation strength during post-sleep sessions (see Methods) was higher for social-discriminант than for non-discriminант assemblies in CA1 ($P=0.043$, rank-sum test) and CA2 ($P=0.0032$) but not CA3 ($P=0.6837$).

recent spatial experience^{1,2,4,7,20,21}. To explore whether social firing was also reactivated during SWRs, we compared the firing correlations of all pairs of hippocampal neurons during social exploration with the correlations during SWRs in both post-sleep and pre-sleep sessions (Fig. 3a). To quantify the correlation between firing during experience and sleep, we adopted the 'explained variance' method (Extended Data Fig. 8a; see Methods)^{21,22}, which was used previously to assess reactivation of CA1 neurons following spatial exploration^{21,22}. As a measure of chance levels, we calculated the reverse explained variance (REV) (see Methods).

Using this method, we found significant levels of reactivation in CA1 and CA2, but not CA3, during post-sleep session SWRs (Fig. 3b). Moreover, optogenetic disruption of SWRs, but not random stimulation, abolished this reactivation (Extended Data Fig. 8b). We also observed significant levels of reactivation when we calculated explained variance on the basis of neural firing throughout the entire non-REM sleep period, not just during SWRs. However, there was no significant reactivation during REM sleep epochs (Extended Data Fig. 8c, d), in line with previous reports^{21,22}.

We found similar region-specific patterns of reactivation when we analysed a subsample of cells of equal number in each region (Extended

Data Fig. 8e). Of further interest, social-remapping cells had higher explained variance values than social-invariant cells in both CA2 and the other areas (Fig. 3c and Extended Data Fig. 8f, g), indicating the preferential reactivation of cells encoding social representations following social experience.

We hypothesized that groups of cells that are co-active during a social-exploration episode might form functional assemblies that are reactivated during SWRs, in a manner similar to the reactivation of place-cell assemblies representing experienced trajectories^{1,2,4,7,20,21}. To test this idea, we used a previously developed approach to identify assemblies of co-active neurons during social exploration^{20,23} (Fig. 3d and Methods). When examined during the learning trials, CA2 and CA1, but not CA3, cell assemblies were more strongly activated during periods of social interaction than at other times during the trials (Fig. 3e and Extended Data Fig. 9a–c). Of particular interest, some assemblies, termed 'social-discriminант assemblies' (see Methods), were activated more during interactions with one stimulus mouse than with the other (Fig. 3f and Extended Data Fig. 9b). Moreover, discriminant assemblies were more abundant in CA2 than in CA1 or CA3 (Fig. 3g).

Next, we explored whether cell assemblies identified during the social-learning trials were reactivated during post-sleep SWRs

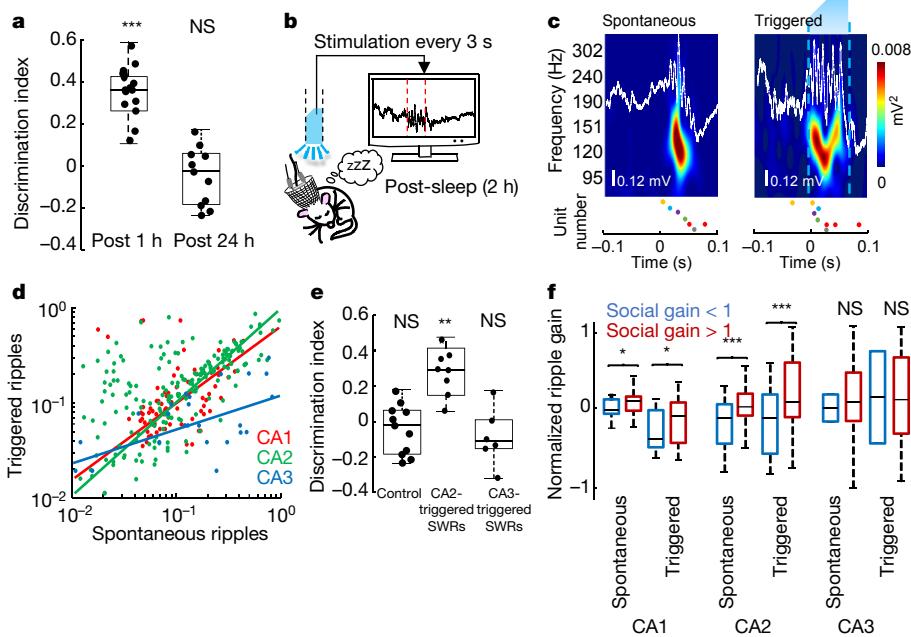


Fig. 4 | Effect of optogenetic generation of ripples on social-memory recall.

a, Social-memory recall was present 1 h (same data as control group in Fig. 1j; discrimination index > 0 ; $P < 0.001$, t -test) but absent 24 h after social-learning trials ($n = 11$ sessions in $n = 6$ mice; $P > 0.05$, t -test). **b**, ChR2 activation in CA2 neurons of Amigo2-Cre mice with low-intensity blue-light pulses triggered ripples in CA2 during the first 2 h of the post-sleep session. **c**, Example of spontaneous and triggered CA2 ripples and spiking from one animal. White lines show CA2 LFPs (scale bar below, 0.12 mV); colour maps show wavelet spectrograms; the pale blue shape at the top indicates the light stimulus. The firing of colour-coded units is shown in the raster plots at bottom. **d**, Correlation of the probability of participation (see Methods) in spontaneous versus triggered CA2 ripples for CA1 ($n = 67$; $r = 0.56$, $P < 10^{-3}$), CA2 ($n = 147$; $r = 0.66$,

$P < 10^{-25}$) and CA3 ($n = 40$; $r = 0.26$, $P > 0.05$) pyramidal cells. **e**, Social memory after 24 h in three groups of mice, all injected with Cre-dependent AAV expressing ChR2 and given blue-light pulses. Control, Cre⁻ littermates. Discrimination index not significantly greater than 0 ($P > 0.05$, sign-rank test, $n = 11$ sessions in $n = 6$ mice). CA2-triggered SWRs, Amigo2-Cre mice expressing ChR2 in CA2 neurons; discrimination index significantly greater than 0 ($P < 0.0002$, $n = 8$ sessions in $n = 6$ mice). CA3-triggered SWRs, Grik4-Cre mice expressing ChR2 in CA3 neurons; discrimination index not significantly greater than 0 ($P > 0.05$, $n = 6$ mice). **f**, Ripple reactivation gain (see Methods) for both spontaneous and triggered SWRs was greater for cells with positive versus negative social gain in CA1 ($P < 0.05$, $n = 67$ cells) and CA2 ($P < 0.003$, $n = 147$ cells) but not CA3 ($P > 0.05$, $n = 40$ cells).

and/or during social interactions in the recall trial. We found substantial reactivation of assemblies in CA1 and CA2 hippocampal regions. Of interest, the strength of reactivation of discriminant assemblies during post-sleep and recall trials was stronger than that of non-discriminatory assemblies (Fig. 3h and Extended Data Fig. 9d–f), suggesting that assemblies encoding more precise social information were preferentially reactivated following social experience. Finally, peri-SWR assembly activation showed a higher activity of discriminant assemblies during SWRs in the sleep session after social learning than before learning (Extended Data Fig. 9d–f). These results suggest that hippocampal cell ensembles, preferentially from the CA2 region, encode a representation of conspecifics that is reactivated during sleep.

Triggered CA2 SWRs extend social memory

To determine whether reactivation of social assemblies during sleep is important for consolidation of social memory, we investigated whether triggering additional SWRs in CA2 in the post-sleep period after social learning could enhance social-memory recall. Optogenetic stimulation with appropriately shaped light pulses of CA1 pyramidal cells expressing ChR2 has been shown to trigger ripple oscillations^{8,24,25}. Furthermore, optogenetic prolongation of CA1 SWRs during a spatial working memory task can improve memory performance⁸. To allow us to detect an enhancement in memory, we used a more demanding social-memory task with a 24-hour delay interval (instead of 1-hour interval), where memory performance was initially at chance levels (Fig. 4a).

To examine the effect of induced SWRs, we expressed ChR2 in CA2 pyramidal cells and applied weak (1–1.5 mW), 60–70-millisecond trapezoidal-shaped light pulses, which triggered ripples with features

similar to spontaneous events (Fig. 4b, c; refs. ^{8,24,25}). This protocol produced a roughly twofold increase in the number of ripples in the first 2 hours of the 24-hour delay period relative to control mice (Extended Data Fig. 10b). Both a neuron's firing rate during a ripple and its probability of firing in a ripple were similar for spontaneous compared with evoked ripples in CA1, CA2 and CA3 (Fig. 4d and Extended Data Fig. 10c, d), in agreement with prior results for CA1 (refs. ^{8,24}). Notably, the increase in ripple number following social exposure resulted in a significant social memory 24 hours after learning (Fig. 4e). By comparison, there was no effect of the light pulses to enable social memory in the Cre-negative, virus-injected control group (Extended Data Fig. 10e).

We next investigated whether the strength of reactivation of a cell within spontaneous or optogenetically triggered ripples was influenced by the degree to which that cell showed socially related firing during the social learning trials. We classified the social firing of each cell by its 'social gain', as follows: (firing rate during social interactions – firing rate outside of social interactions)/(sum of the rates). We found that cells with a positive social gain had a greater 'ripple reactivation gain' – the extent to which firing rate during post-sleep ripples was increased relative to pre-sleep ripples (Fig. 4f). Cells with positive social gain also displayed a higher probability of participation in both spontaneous and triggered SWRs (Extended Data Fig. 10f). Thus, we conclude that SWRs are privileged windows for learning-related changes in excitability owing to their intrinsic or synaptic plasticity²⁶ properties, as previously suggested²⁷.

Finally, we examined whether the optogenetic enhancement of social memory was specific to SWRs triggered in CA2, or whether the generation of SWRs in neighbouring CA3 could produce a similar effect. We thus expressed ChR2 in CA3 pyramidal cells by injecting Cre-dependent AAV in CA3 of Grik4-Cre²⁸ mice (Extended Data Fig. 10g, h). Although

photostimulation of CA3 generated SWRs (Extended Data Fig. 10i–k), it failed to improve social-memory recall after 24 hours (Fig. 4e). Of interest, CA3-triggered SWRs recruited the firing of pyramidal neurons in CA3 and CA1 but not in CA2 (Extended Data Fig. 10l–n), suggesting that CA2 firing activity during SWRs is essential for social-memory consolidation. This is consistent with results showing that dorsal CA2^{10–12,29}, but not dorsal CA1³⁰ or dorsal CA3³¹, is crucial for social memory, and that activation of CA3 produces a net feedforward inhibition in CA2³².

Discussion

Our results extend previous findings that SWRs replay spatial trajectories by providing evidence that SWRs also reactivate and consolidate higher-order multimodal experiences encoded in social memory. Furthermore, our findings suggest that SWRs originating from different regions may have different functional roles: CA3 SWRs seem to be important for spatial memory^{7,33}, whereas consolidation of social memory requires SWRs arising in CA2.

These results also further our understanding of how CA2 activity contributes to social memory. Thus, whereas dorsal CA2 firing has been found to respond to and encode social novelty^{12,29}, our finding of ‘social-remapping’ place cells indicates that dorsal CA2 neurons encode representations that can distinguish the identity of one novel mouse from another. These results are consistent with studies of humans showing that individual neurons in the medial temporal lobe respond to the identity of a given individual^{34,35}, suggesting that hippocampal function in social memory is conserved through evolution.

By comparing the firing properties and behavioural role of neurons in different hippocampal regions, we provide further support that these regions are preferentially involved in distinct functions. Thus, whereas social-remapping cells were enriched in dorsal CA2, object-remapping cells were enriched in dorsal CA1 and CA3. Notably, this preferential neural coding was reflected in memory behaviour, with CA2 important for social memory and CA1 for object memory. This is consistent with previous findings that social memory requires dorsal CA2^{10,11,29} but not dorsal CA1³⁰ or dorsal CA3³¹.

As dorsal CA1 does not seem to be essential for social memory, what is the circuit mechanism by which dorsal CA2 output enables social-memory formation? Insight into this question comes from the finding that ventral CA1—which, like dorsal CA1, also receives strong excitatory input from dorsal CA2^{11,36}—is important for social memory³⁰. Moreover, silencing the longitudinal inputs to ventral CA1 from dorsal CA2 is sufficient to impair social memory¹¹. It will be interesting to test whether SWRs originating in dorsal CA2 travel to ventral CA1 to consolidate social memory at this site, as suggested by the finding of an increased number of SWRs in ventral CA1 in the presence of conspecifics³⁷. Finally, although the role of dorsal CA2 output to dorsal CA1 remains uncertain, this pathway is poised to contribute to the finding that some place cells in dorsal CA1 encode the allocentric position of a freely moving conspecific, and thereby serve as social place cells^{38,39}. Thus, dorsal CA2—through both its encoding of social experience and its replay of that experience—can contribute to a wide range of social-behaviour and social-information processing in the brain.

Online content

Any methods, additional references, Nature Research reporting summaries, source data, extended data, supplementary information, acknowledgements, peer review information; details of author contributions and competing interests; and statements of data and code availability are available at <https://doi.org/10.1038/s41586-020-2758-y>.

1. Wilson, M. A. & McNaughton, B. L. Reactivation of hippocampal ensemble memories during sleep. *Science* **265**, 676–679 (1994).
2. Karlsson, M. P. & Frank, L. M. Awake replay of remote experiences in the hippocampus. *Nat. Neurosci.* **12**, 913–918 (2009).

3. Girardeau, G., Benchenane, K., Wiener, S. I., Buzsáki, G. & Zugaro, M. B. Selective suppression of hippocampal ripples impairs spatial memory. *Nat. Neurosci.* **12**, 1222–1223 (2009).
4. Dupret, D., O’Neill, J., Pleydell-Bouverie, B. & Csicsvari, J. The reorganization and reactivation of hippocampal maps predict spatial memory performance. *Nat. Neurosci.* **13**, 995–1002 (2010).
5. Ego-Stengel, V. & Wilson, M. A. Disruption of ripple-associated hippocampal activity during rest impairs spatial learning in the rat. *Hippocampus* **20**, 1–10 (2010).
6. Jadhav, S. P., Kemere, C., German, P. W. & Frank, L. M. Awake hippocampal sharp-wave ripples support spatial memory. *Science* **336**, 1454–1458 (2012).
7. Buzsáki, G. Hippocampal sharp wave-ripple: a cognitive biomarker for episodic memory and planning. *Hippocampus* **25**, 1073–1188 (2015).
8. Fernández-Ruiz, A. et al. Long duration hippocampal sharp wave ripples improve memory. *Science* **364**, 1082–1086 (2019).
9. Oliva, A., Fernández-Ruiz, A., Buzsáki, G. & Berényi, A. Role of hippocampal CA2 region in triggering sharp-wave ripples. *Neuron* **91**, 1342–1355 (2016).
10. Hitti, F. L. & Siegelbaum, S. A. The hippocampal CA2 region is essential for social memory. *Nature* **508**, 88–92 (2014).
11. Meira, T. et al. A hippocampal circuit linking dorsal CA2 to ventral CA1 critical for social memory dynamics. *Nat. Commun.* **9**, 4163 (2018).
12. Alexander, G. M. et al. Social and novel contexts modify hippocampal CA2 representations of space. *Nat. Commun.* **7**, 10300 (2016).
13. Kay, K. et al. A hippocampal network for spatial coding during immobility and sleep. *Nature* **531**, 185–190 (2016).
14. Rubin, A., Yartsev, M. M. & Ulanovsky, N. Encoding of head direction by hippocampal place cells in bats. *J. Neurosci.* **34**, 1067–1080 (2014).
15. Gerfen, C. R., Paletzki, R. & Heintz, N. GENSAT BAC cre-recombinase driver lines to study the functional organization of cerebral cortical and basal ganglia circuits. *Neuron* **80**, 1368–1383 (2013).
16. Knierim, J. J., Lee, I. & Hargreaves, E. L. Hippocampal place cells: parallel input streams, subregional processing, and implications for episodic memory. *Hippocampus* **16**, 755–764 (2006).
17. Eschenko, O., Ramadan, W., Mölle, M., Born, J. & Sara, S. J. Sustained increase in hippocampal sharp-wave ripple activity during slow-wave sleep after learning. *Learn. Mem.* **15**, 222–228 (2008).
18. Alexander, G. M. et al. CA2 neuronal activity controls hippocampal low gamma and ripple oscillations. *eLife* **7**, e38052 (2018).
19. Boehringer, R. et al. Chronic loss of CA2 transmission leads to hippocampal hyperexcitability. *Neuron* **94**, 642–655 (2017).
20. van de Ven, G. M., Trouche, S., McNamara, C. G., Allen, K. & Dupret, D. Hippocampal offline reactivation consolidates recently formed cell assembly patterns during sharp-wave ripples. *Neuron* **92**, 968–974 (2016).
21. Kudrimoti, H. S., Barnes, C. A. & McNaughton, B. L. Reactivation of hippocampal cell assemblies: effects of behavioral state, experience, and EEG dynamics. *J. Neurosci.* **19**, 4090–4101 (1999).
22. Girardeau, G., Inema, I. & Buzsáki, G. Reactivations of emotional memory in the hippocampus-amygdala system during sleep. *Nat. Neurosci.* **20**, 1634–1642 (2017).
23. Lopes-dos-Santos, V., Ribeiro, S. & Tort, A. B. L. Detecting cell assemblies in large neuronal populations. *J. Neurosci. Methods* **220**, 149–166 (2013).
24. Stark, E., Roux, L., Eichler, R. & Buzsáki, G. Local generation of multineuronal spike sequences in the hippocampal CA1 region. *Proc. Natl. Acad. Sci. USA* **112**, 10521–10526 (2015).
25. Oliva, A., Fernández-Ruiz, A., Fermino de Oliveira, E. & Buzsáki, G. Origin of gamma frequency power during hippocampal sharp-wave ripples. *Cell Rep.* **25**, 1693–1700 (2018).
26. King, C., Henze, D. A., Leinekugel, X. & Buzsaki, G. Hebbian modification of a hippocampal population pattern in the rat. *J. Physiol.* **521**, 159–167 (1999).
27. Grosmark, A. D. & Buzsáki, G. Diversity in neural firing dynamics supports both rigid and learned hippocampal sequences. *Science* **351**, 1440–1443 (2016).
28. Wagatsuma, A. et al. Locus coeruleus input to hippocampal CA3 drives single-trial learning of a novel context. *Proc. Natl. Acad. Sci. USA* **115**, E310–E316 (2018).
29. Donegan, M. L. et al. Coding of social novelty in the hippocampal CA2 region and its disruption and rescue in a 22q11.2 microdeletion mouse model. *Nat. Neurosci.* <https://doi.org/10.1038/s41593-020-00720-5> (2020).
30. Okuyama, T., Kitamura, T., Roy, D. S., Itohara, S. & Tonegawa, S. Ventral CA1 neurons store social memory. *Science* **353**, 1536–1541 (2016).
31. Chiang, M. C., Huang, A. J. Y., Wintzer, M. E., Ohshima, T. & McHugh, T. J. A role for CA3 in social recognition memory. *Behav. Brain Res.* **354**, 22–30 (2018).
32. Chevaleyre, V. & Siegelbaum, S. A. Strong CA2 pyramidal neuron synapses define a powerful disynaptic cortico-hippocampal loop. *Neuro* **66**, 560–572 (2010).
33. Davoudi, H. & Foster, D. J. Acute silencing of hippocampal CA3 reveals a dominant role in place field responses. *Nat. Neurosci.* **22**, 337–342 (2019).
34. Quiroga, R. Q., Reddy, L., Kreiman, G., Koch, C. & Fried, I. Invariant visual representation by single neurons in the human brain. *Nature* **435**, 1102–1107 (2005).
35. Rey, H. G. et al. Single neuron coding of identity in the human hippocampal formation. *Curr. Biol.* **30**, 1152–1159 (2020).
36. Tamamaki, N., Abe, K. & Nojyo, Y. Three-dimensional analysis of the whole axonal arbors originating from single CA2 pyramidal neurons in the rat hippocampus with the aid of a computer graphic technique. *Brain Res.* **452**, 255–272 (1988).
37. Rao, R. P., von Heimendahl, M., Bahr, V. & Brecht, M. Neuronal responses to conspecifics in the ventral CA1. *Cell Rep.* **27**, 3460–3472 (2019).
38. Omer, D. B., Maimon, S. R., Las, L. & Ulanovsky, N. Social place-cells in the bat hippocampus. *Science* **359**, 218–224 (2018).
39. Danjo, T., Toyoizumi, T. & Fujisawa, S. Spatial representations of self and other in the hippocampus. *Science* **359**, 213–218 (2018).

Publisher’s note Springer Nature remains neutral with regard to jurisdictional claims in published maps and institutional affiliations.

© The Author(s), under exclusive licence to Springer Nature Limited 2020

Methods

Surgical procedures

Adult male mice (C57Bl6/J background, roughly 3 months old) were kept in a vivarium on a 12-hour light/dark cycle; before surgery, three to four animals were housed per cage; after surgery, animals were housed individually. All experiments were approved by the Institutional Animal Care and Use Committee at Columbia University. We used Cre-dependent AAV injections to obtain region-selective expression of opsins in hippocampal CA2 (Amigo2-Cre animals¹⁰), CA3 (Grik4-Cre animals²⁸) or CA1 (Lypd1-Cre animals¹⁵) regions for optogenetic manipulations.

Following anaesthesia with isoflurane, a craniotomy was performed through stereotaxic guidance over the target region, and animals were bilaterally injected with AAV2/5 EF1a.DIO.hChR2.eYFP or AAV2/5 EF1a.DIO.eArch3.0-eYFP (200 nl per site) using a Nanoject II (Drummond Scientific). After injections, the skin was sutured and animals were treated with a broad-spectrum antibiotic and given an analgesic. Animals were left in the vivarium for recovery (roughly two weeks).

One week later, animals were implanted unilaterally with silicon probes (-1.94 anteroposterior, -2.2 mediolateral from Bregma) and bilaterally with optic fibres (-1.94 anteroposterior, ± 2.2 mediolateral), similar to published procedures^{8,9,25,39}. In a subset of behavioural experiments, animals were implanted with optic fibres only. The probes (five shanks \times 12 sites $-A5 \times 12$ -Poly 2–5 mm 20 s-160-, or four shanks \times 16 sites $-A4 \times 16$ Poly 2–5 mm 20 s-160-; Neuronexus) were mounted on custom-made micro-drives to allow their vertical movement following implantation. A fibre optic was attached under microscopic guidance to one of the shanks of the silicon probe. Probes were inserted above the target region and the microdrives were attached to the skull with dental cement. In the contralateral hemisphere, an optic fibre (200 μ m) was implanted over the target region and cemented to the skull. For animals implanted with fibre optics only, both fibres were implanted in the final position and attached to the skull with dental cement. Craniotomies were sealed with sterile wax. A stainless-steel wire was inserted over the cerebellum to serve as ground and reference for the recordings. Finally, a copper mesh was attached to the skull to strengthen the implant and connected to the ground wire to attenuate the contamination of the recordings by environmental electrical noise. After post-surgery recovery (roughly one week), probes were lowered gradually in 75–150- μ m steps per day until the desired position was reached. We used physiological landmarks and characteristic LFP patterns^{40–42} to identify the pyramidal layer of the different subregions of the hippocampus^{40–42} and optogenetic responses.

Optogenetic experiments

For real-time SWR manipulations, 100- or 200- μ m-core multimode optic fibres (Thor Labs) were collimated to a blue-light-emitting (475 nm) laser diode (PL-450, Osram) connected to current source stimulators (Thor Labs)^{8,24,25,43}. For the stimulation session, these diodes were connected to the implanted fibres.

SWR disruption. A closed-loop system was used to detect SWRs online and to trigger light stimulation. For SWR disruption, once a ripple was detected, a short duration (10 ms) high-intensity (5–10 mW) light pulse was delivered through both fibres to activate ChR2 (ref. ⁸). The intensity was manually adjusted in each animal during test sessions in the home cage by gradually increasing light power until a population spike was evoked, truncating the ongoing ripple and producing a strong inhibition of pyramidal cell firing, similar to the effect of electrical stimulation^{3,5,6}. Pulses were delivered every time a ripple was detected while the animal was in the home cage, between the learning and the recall trial. Two control stimulation experiments were performed. The first control group consisted of Cre⁺ animals expressing ChR2 as above and received the same light stimulation upon SWR detection, but after a

random delay (500–1,000 ms). The second control group consisted of Cre⁻ animals which were injected with the same Cre-dependent ChR2 AAV as above and received the same light stimulation upon SWR detection as the experimental group. The performance of the protocol was validated with a subsample of the data to determine the rate of positive detections (hits), false positives (false alarms) and missed events (Extended Data Fig. 7b).

SWR generation. For SWR generation, 60-ms, low-intensity (1–2 mW) light pulses were used to activate ChR2 (refs. ^{8,24,25}). The intensity was manually adjusted during a test session in the home cage by gradually increasing light power until a ripple was produced. To minimize the artefact at the onset of the stimulation, trapezoid-shaped pulses (roughly 20-ms initial ramp) were used. Pulses were delivered constantly at a rate that approximated the spontaneous occurrence of SWRs (0.3 Hz). Control stimulation experiments were performed using the same virus and stimulation protocol in Cre⁻ animals.

Pyramidal cell silencing during SWRs in sleep. For the SWR silencing experiments, a yellow laser (556 nm, Opto-Engine-LLC) delivered light (3–5 mW light pulses, each for 30 s, once every 2 min) to activate eArch3.0 (ref. ⁴³). For controls, the same stimulation was applied to Cre⁻ animals.

Pyramidal cell silencing during social interactions. We expressed eArch3.0 selectively in CA1 or CA2 by using Cre-dependent AAV injections in these regions in Lypd1-Cre or Amigo2-Cre mice, respectively. For real-time behavioural manipulations, we streamed online (<https://github.com/wonkoderverstaendige/Spotter>) the position of the animals during learning trials 1 and 2. Yellow light pulses (5 mW) were delivered continuously to activate eArch3.0 (ref. ⁴³) when the animals crossed into the area of interest around a given stimulus animal.

Pyramidal cell silencing during object interactions. We used the same viruses, animal models and stimulation protocol as above (in the subsection ‘Pyramidal cell silencing during social interactions’). Light pulses were delivered when the animals crossed the area of interest around a given object.

Behavioural recordings

After surgery, animals were handled daily and accommodated to the experimenter, the recording room, the recording cable and the recording arena for one week before starting experiments. In a typical session we recorded neural activity as follows: 1 h in the home cage, 5 min during exposure to the empty arena, 1 h in the home cage, 5 min during exposure to the empty cup cages, 1 h in the home cage (pre-sleep), 5 min during exposure to the two novel stimulus animals (S_1 and S_2) in the learning trial 1, 5 min during exposure to the same stimulus mice in reversed positions in learning trial 2, 1 h in the home cage (post-sleep, where SWRs manipulations were performed in some sessions), and a 5-min recall trial, during which one of the two stimulus mice (S_1 or S_2 , chosen at random) was presented together with a novel stimulus animal (N). Analogous procedures were followed for the object-recognition experiments, with different objects being a piece of cork, wood, plastic, glass or rubber (all about 10 cm tall and 5 cm \times 5 cm wide). For the 24-h recall experiment, the recall test was conducted on the next day. Adult (roughly three-month-old) C57Bl6/J non-littermate males were used as stimulus animals.

The position of the animal was tracked online using two LEDs (one blue and one red) and an overhead camera (Basler, 60 Hz). Offline tracking of the animal was validated using pose estimation user-defined features with a deep learning algorithm (<https://github.com/AlexEMG/DeepLabCut>)⁴⁴. In each trial we measured the total time the subject mouse spent exploring the two stimulus mice (t_{S1}, t_{S2}) in the two learning trials, and the differential time spent in social exploration of the

Article

stimulus mouse (for example, t_{S1}) compared with the novel mouse (t_N) in the recall trial (or the novel object in the case of the object experiments). The differential interaction was quantified by a discrimination index. When S_1 was presented in the recall trial, the discrimination index was defined as $(t_N - t_{S1})/(t_N + t_{S1})$, with an analogous expression when S_2 was presented. Social exploration was defined as time spent inside the interaction zone (considered to an area within 5 cm of the perimeter of the cup).

Electrophysiological recordings were conducted using an Intan RHD2000 interface board (http://intantech.com/RHD_USB_interface_board.html) at 20 kHz sampling.

Real-time SWR detection

Two LFP channels were used for real-time SWR detection^{8,25}. The ripple was detected in one channel connected to an electrode in the CA2 region, previously identified by optogenetic tagging of a cell's response. The LFP was filtered between 100 Hz and 300 Hz. A second channel was used for noise detection, selected from the neocortex where no ripple activity was present and filtered in the same frequency band. The root-mean square (r.m.s.) of the two signals was computed using a custom-made analogue circuit. Signals were fed into a data-acquisition interface for real-time processing of LFP channels by a programmable processor (Cambridge Electronic Design) at a 20-kHz sampling rate. Amplitude thresholds for ripple versus noise were manually adjusted for each animal before the start of each recording session on the basis of physiological features. SWRs were defined as events crossing the ripple detection but not the noise signal detection^{8,25}.

Tissue processing and immunohistochemistry

Mice were transcardially perfused with saline followed by 4% paraformaldehyde (PFA) in phosphate-buffered saline (PBS). The brains were quickly extracted and incubated in 4% PFA overnight. After 1 h of washing in 0.3% glycine in PBS, 60-μm sections were prepared using a Leica VT1000S vibratome. Sections were permeabilized and blocked for 2 h at room temperature in PBS containing 5% goat serum and 0.5% Triton-X. Sections were incubated overnight at 4 °C with chicken anti-GFP primary antibody (1:1,000, Aves Labs, catalogue number GFP-1020; Resource Identification Portal (RRID; <https://scicrunch.org/resources>) identification code AB_10000240) and rabbit anti-PCP4 primary antibody (1:200, Sigma-Aldrich, catalogue number HPA005792; RRID code AB_1855086), diluted in PBS containing 5% goat serum and 0.1% Triton-X in PBS. The sections were washed three times for 15 min in PBS at room temperature and secondary antibodies were applied overnight at 4 °C in PBS containing 5% goat serum and 0.1% Triton-X. All secondary antibodies were raised in goats and purchased from ThermoFisher Scientific. The secondary incubation was performed with anti-chicken antibody conjugated to Alexa 488 (catalogue number A11039; RRID AB_142924) and anti-rabbit antibody conjugated to Alexa 647 (catalogue number A21244; RRID AB_2535812). Slices were stained with DAPI (ThermoFisher Scientific, catalogue number D9542) applied at 1:1,000 for 10 min in PBS at room temperature before mounting the section using fluoromount (Sigma-Aldrich). An inverted confocal microscope (Zeiss, LSM 700) was used for fluorescent imaging and quantification of virus expression. Animals were discarded if fewer than 80% of cells in a given subregion expressed a given viral construct. According to this criterion, five Lypd1-Cre animals did not fully express virus in CA1 and were discarded. All other animals met the criterion. An epifluorescence microscope (Olympus BX61VS) was used to verify the tracks of electrodes and optical fibres.

Quantification and statistical analysis

Spike sorting and unit classification. Neuronal spikes were detected from the digitally high-pass-filtered LFP (0.5–5 kHz) by a threshold-crossing-based algorithm (Spikedetekt2). Detected spikes were semi-automatically sorted using Kilosort (<https://github.com/cortex-lab/>

KiloSort), followed by manual curation using Phy (<https://github.com/kwikteam/phy>)⁴⁵. Autocorrelograms and waveforms characteristic of monosynaptic excitatory and inhibitory interactions were used to select and characterize well isolated units and separate them into pyramidal cell and interneuron classes^{9,46}. Only well isolated single units were included.

Offline detection of SWRs. For detection of ripples, the wide-band signal was band-pass filtered (using difference-of-Gaussians, with a zero-lag, linear-phase finite impulse response (FIR)), and instantaneous power was computed by clipping at four standard deviations from the mean, then rectified and low-pass filtered. The low-pass filter cut-off was at a frequency corresponding to n cycles of the mean band-pass (for a band pass at 100–300 Hz, the low-pass was 55 Hz). The mean and standard deviation of the LFP baseline were computed on the basis of the power during non-REM sleep. Subsequently, the power of the non-clipped signal was computed, and all events exceeding four standard deviations from the mean were detected. Events were then expanded until the (non-clipped) power fell below one standard deviation; short events (of less than 15 ms) were discarded^{8,9,24,25}.

Ripple spike content analysis. Well isolated putative units with at least 100 spikes in a given session were included in the analysis. For all individual units, spikes in a [-300, +300]-ms peri-ripple or stimulus onset window were collected and firing rate histograms (1-ms time bins) were constructed. All histograms for the same subregions and same type of units (pyramidal cells) were pooled. The firing rate histograms were z-scored and smoothed using a Gaussian kernel (one standard deviation = 5 ms). Only spikes that were within the interval of the detected ripples were considered for the ripple content analysis. The in-ripple firing rate was calculated as the number of spikes divided by the ripple duration, and averaged for all events. The probability of participation of individual units in ripples was defined as the number of events in which a neuron fired at least one spike during the ripple, divided by the total number of ripples. Within-ripple gain was calculated as in-ripple firing rate divided by the baseline firing rate (average firing rate in the whole session) of the cell^{8,24,25}.

Reactivation analysis. The explained variance (EV) and reverse explained variance (REV) were calculated in each session using cell pairs of interest, for pyramidal cells only, using a previously described approach^{21,22}. For the explained variance:

$$\text{EV} = r_{\text{social episode, POST, PRE}}^2 \\ = \left(\frac{r_{\text{social episode, POST}} - r_{\text{social episode, PRE}} \times r_{\text{POST, PRE}}}{\sqrt{(1 - r_{\text{social episode, PRE}}^2) - (1 - r_{\text{POST, PRE}}^2)}} \right)^2$$

where $r_{\text{social episode, POST}}$ and $r_{\text{social episode, PRE}}$ are the Pearson's correlation coefficients of pairwise correlation matrices between the social learning episodes and SWR times of the post-sleep and pre-sleep periods, respectively, and $r_{\text{POST, PRE}}$ is the Pearson's correlation coefficient of the pairwise correlation matrices between the post-sleep and pre-sleep periods. For measurement of EV and REV during REM sleep, non-REM sleep and SWRs, all epochs/events were detected individually and pooled together in both pre- and post-sleep periods. Pairwise neuronal correlations for EV and REV were calculated using the Pearson's correlation coefficient on 100-ms binned spike trains. The coefficients were calculated for pre-sleep, task and post-sleep periods separately and correlation matrices were then computed. The correlations between all pairwise combinations were calculated and used to assess the percentage of variance in the post-sleep period that could be explained by correlation values established during the task trials, while controlling for pre-existing correlations in the pre-sleep session. The control value (REV) was obtained by switching

the temporal order of the pre- and post-sleep sessions. For assessment of the relative contribution to the explained variance of a single pair of neurons, the EV was calculated for all of the pairs without including the pair of interest. Subtracting this value from the total EV value, the relative contribution of the corresponding pair of neurons could be calculated. To calculate the average contribution of each neuron to the EV, we averaged the relative contribution of all pairs in which a particular neuron participated²².

To detect cell assembly patterns, we used an unsupervised statistical framework based on a hybrid principal component analysis (PCA) followed by independent component analysis (ICA) as described^{20,23}. In brief, spike trains of each neuron were binned in 20-ms intervals for the whole session, and z-scored firing rates were calculated for each bin. Spike trains were convolved with a Gaussian kernel (standard deviation = 10 ms), and the matrix of firing correlation coefficients for all pairs of neurons was constructed. Next, we calculated the number of assemblies based on those principal components whose eigenvalues exceeded the threshold for random firing correlations (Marčenko–Pastur distribution). ICA was then used to determine for each assembly (component) the vector of weights with which each neuron's firing contributes to that assembly. To measure the strength of each assembly's activation as a function of time in a given episode, we multiplied the convolved z-scored firing rate of a given neuron at a given time by the weight of that neuron's contribution to a given assembly. We then summed the product of these weighted spike counts for all non-identical pairs of neurons to provide the assembly activation strength at the given time point. Assembly activity was considered only when its expression strength exceeded a threshold of 5 (ref. ²³). The reactivation strength of an assembly was defined as the difference in its average expression strength during post-sleep minus that during pre-sleep. Larger reactivation numbers indicate a greater social-learning-dependent increase in assembly activation. Assembly activation was assessed inside and outside the two social-interaction areas surrounding the stimulus mice. Social-discriminant assemblies were defined as assemblies that were activated significantly more strongly during the interaction with one of the two stimulus mice compared with the other one in the two learning trials ($P < 0.05$, Student's *t*-test).

Place cells and analysis. Spiking data were binned into 1-cm-wide segments of the camera field projected onto the maze floor, generating raw maps of spike counts and occupancy probability. A Gaussian kernel (standard deviation = 5 cm) was applied to both raw maps of spike and occupancy, and a smoothed rate map was constructed by dividing the spike map by the occupancy map. A place field was defined as a continuous region of at least 15 cm², where the mean firing rate was greater than 10% of the peak rate in the maze, the peak firing rate was greater than 2 Hz, and the spatial coherence was larger than 0.7. Spatial correlation between trials was calculated as the average pixel-by-pixel correlation of the smoothed firing-rate maps. The rotated spatial correlation was calculated in the same way but rotating by 180° the rate map in trial 2, so that the positions of mice S₁ and S₂ matched those of trial 1; a similar procedure was used in the object experiments. The distance of each place field to the cups (or objects) was calculated from the centre of mass of the field to the centre of the closest cup. Information index per spike (bits per spike) represents the mean firing rate of the cell at location X , multiplied by the probability of the animal of being at location X and the binary logarithm of the mean firing rate of the cell at location X divided by the overall firing rate of the cell^{47,48}. The selectivity index represents the maximum firing rate of the rate map (spikes divided by time spent in each bin of 5 cm), divided by the mean firing rate^{47,48}.

For the classification of social-invariant and social-remapping cells (and, similarly, object-remapping cells), *k*-means clustering was performed with all normal and rotated correlation values for

all pyramidal cells active during the trials of the task. The 'cityblock' metric was used as a distance measure. Using the silhouette criterion, we found the optimal number of clusters in the data to be five. To be able to classify cells as social-remapping versus social-invariant, we focused on those cells with high rotated versus unrotated correlation values and vice versa (as described above). Most of the cells in these two groups had single place fields away from the centre of the arena (about 48% of all place cells); of the remaining groups (neither 'social-invariant' nor 'social-remapping'), about 13% of cells had place fields in the centre.

Immobility and speed-modulation analysis. Locomotion periods with a speed of less than 4 cm s⁻¹ were considered 'immobility' periods. We excluded immobility periods in which SWRs occurred^{9,13}. For the analyses herein, we considered only those immobility periods that occurred during the behavioural task (not the home cage). For the speed-modulation analysis, spike-count vectors divided by the time spent in each speed bin (1 cm s⁻¹) were calculated and smoothed with a Gaussian kernel of six standard deviations^{9,13,14,48}.

Head-direction analysis. The head direction of the animal was estimated with head markers used for pose estimation⁴⁴. Head-direction fields were calculated as spike-count histograms divided by the time spent in each direction in bins of 2 degrees, smoothed with a Gaussian kernel of six standard deviations. A Rayleigh test was used to test the null hypothesis of head-direction firing being uniformly distributed in all directions^{14,49,50}. The proportion of modulated cells was quantified as those cells modulated with a *P*-value of less than 0.05.

Theta-modulation analysis. For detecting periods of theta activity, LFPs from the pyramidal layer were band-pass filtered (at 4–12 Hz)^{9,40,51}. Peaks were identified as the positive to negative zero crossings of the time derivative of the filtered LFP. Phase was linearly interpolated between peaks^{9,40}. Theta-modulation strength was calculated as the mean resultant angle of the phases (mean vector length), and the null hypothesis of phases being equally distributed was assessed with a Rayleigh test⁵⁰. The proportion of modulated cells was quantified as those cells modulated with *P*-values of less than 0.05.

Statistical analysis

All statistical analyses were performed using Matlab functions or custom-made scripts as described^{1–9,20–25}. The unit of analysis was typically single cells, assemblies or SWR events (unless noted as being sessions or animals). Unless otherwise noted, for all statistical analyses we used non-parametric two-tailed Wilcoxon's rank-sum test (equivalent to Mann–Whitney *U*-test) or Wilcoxon signed-rank test. For multiple comparisons, we used Tukey's honesty post hoc test after ANOVA. In box plots, central marks indicate medians; the bottom and top edges indicate the 25th and 75th percentiles respectively; and whiskers extend to the most extreme data points without considering outliers, which were also included in statistical analyses (outliers are considered to be every point greater than $q_3 + w \times (q_3 - q_1)$ or less than $q_1 - w \times (q_3 - q_1)$ (approximately more than 2.7 standard deviations), where w is the maximum whisker length, and q_1 and q_3 are the 25th and 75th percentiles of the sample data, respectively). Owing to constraints of experimental design, the experimenter was not blind to manipulations performed during experiments (that is, optogenetic manipulations). No statistical tests were used to pre-determine sample sizes of the number of animals, but our sample sizes are similar or larger to those in previous studies. The mice for each group were chosen randomly.

Reporting summary

Further information on research design is available in the Nature Research Reporting Summary linked to this paper.

Data availability

Data sets and analytical tools included in this study are available from the corresponding authors upon reasonable request.

40. Fernández-Ruiz, A. et al. Entorhinal-CA3 dual-input control of spike timing in the hippocampus by theta-gamma coupling. *Neuron* **93**, 1213–1226 (2017).
41. Ylinen, A. et al. Sharp wave-associated high-frequency oscillation (200 Hz) in the intact hippocampus: network and intracellular mechanisms. *J. Neurosci.* **15**, 30–46 (1995).
42. Fernández-Ruiz, A., Makarov, V. A., Benito, N. & Herreras, O. Schaffer-specific local field potentials reflect discrete excitatory events at gamma frequency that may fire postsynaptic hippocampal CA1 units. *J. Neurosci.* **32**, 5165–5176 (2012).
43. Roux, L., Hu, B., Eichler, R., Stark, E. & Buzsáki, G. Sharp wave ripples during learning stabilize the hippocampal spatial map. *Nat. Neurosci.* **20**, 845–853 (2017).
44. Mathis, A. et al. DeepLabCut: markerless pose estimation of user-defined body parts with deep learning. *Nat. Neurosci.* **21**, 1281–1289 (2018).
45. Pachitariu, M., Steinmetz, N., Kadir, S., Carandini, M. & Harris, K. D. Fast and accurate spike sorting of high-channel count probes with KiloSort. In *Proc. 29th Advances in Neural Information Processing Systems* (eds Lee, D. D., Sugiyama, M., Luxburg, U. V., Guyon, R. & Garnett, R.) (2016).
46. Mizuseki, K., Sirota, A., Pastalkova, E. & Buzsáki, G. Theta oscillations provide temporal windows for local circuit computation in the entorhinal-hippocampal loop. *Neuron* **64**, 267–280 (2009).
47. Skaggs, W. E., McNaughton, B. L., Wilson, M. A. & Barnes, C. A. Theta phase precession in hippocampal neuronal populations and the compression of temporal sequences. *Hippocampus* **6**, 149–172 (1996).
48. Oliva, A., Fernández-Ruiz, A., Buzsáki, G. & Berényi, A. Spatial coding and physiological properties of hippocampal neurons in the Cornu Ammonis subregions. *Hippocampus* **26**, 1593–1607 (2016).
49. Peyrache, A., Lacroix, M. M., Petersen, P. C. & Buzsáki, G. Internally organized mechanisms of the head direction sense. *Nat. Neurosci.* **18**, 569–575 (2015).

50. Berens, P. CircStat: a MATLAB toolbox for circular statistic. *J. Stat. Softw.* **31**, <https://www.jstatsoft.org/article/view/v031i10> (2009).

51. Fernandez-Lamo, I. et al. Proximodistal organization of the CA2 hippocampal area. *Cell Rep.* **26**, 1734–1746 (2019).

Acknowledgements We thank G. Buzsaki for comments and resource sharing; members of the Siegelbaum laboratory for comments and discussions on the manuscript; and T. Meira for help with designing the behavioural paradigm. This work was supported by the NVIDIA Corporation, an EMBO Postdoctoral Fellowship (ALTF 120-2017) and a K99 grant from the US National Institutes of Health (NIH; K99MH122582) (to A.O.); a Sir Henry Wellcome Postdoctoral Fellowship and K99 grant (K99MH120343) (to A.F.-R.); a National Alliance for Research on Schizophrenia and Depression (NARSAD) Young Investigator award from the Brain and Behavior Foundation founded by the Osterhaus family (to F.L.); and grants MH-104602 and MH-106629 from the National Institute of Mental Health (NIMH) and a grant from the Zegar Family Foundation (to S.A.S.).

Author contributions A.O. and S.A.S. conceptualized the research; A.O. carried out experiments and data collection; A.O. and A.F.-R. analysed data; F.L. carried out immunohistochemistry; A.O. wrote the original draft of the manuscript; A.O. and S.A.S. reviewed and edited the manuscript; A.O., A.F.-R. and F.L. created figures; S.A.S. supervised the research and acquired funding.

Competing interests The authors declare no competing interests.

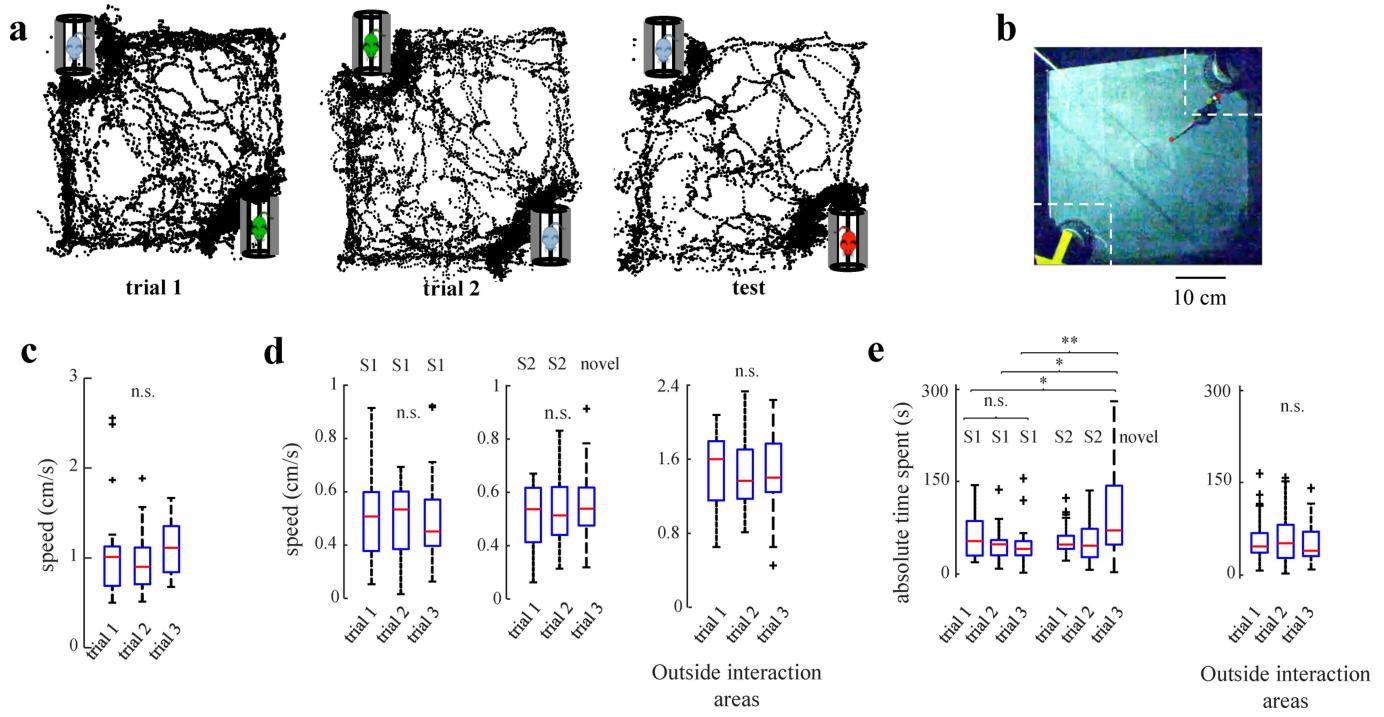
Additional information

Supplementary information is available for this paper at <https://doi.org/10.1038/s41586-020-2758-y>.

Correspondence and requests for materials should be addressed to A.O. or S.A.S.

Peer review information *Nature* thanks Shigeyoshi Fujisawa, Torkel Hafting and the other, anonymous, reviewer(s) for their contribution to the peer review of this work.

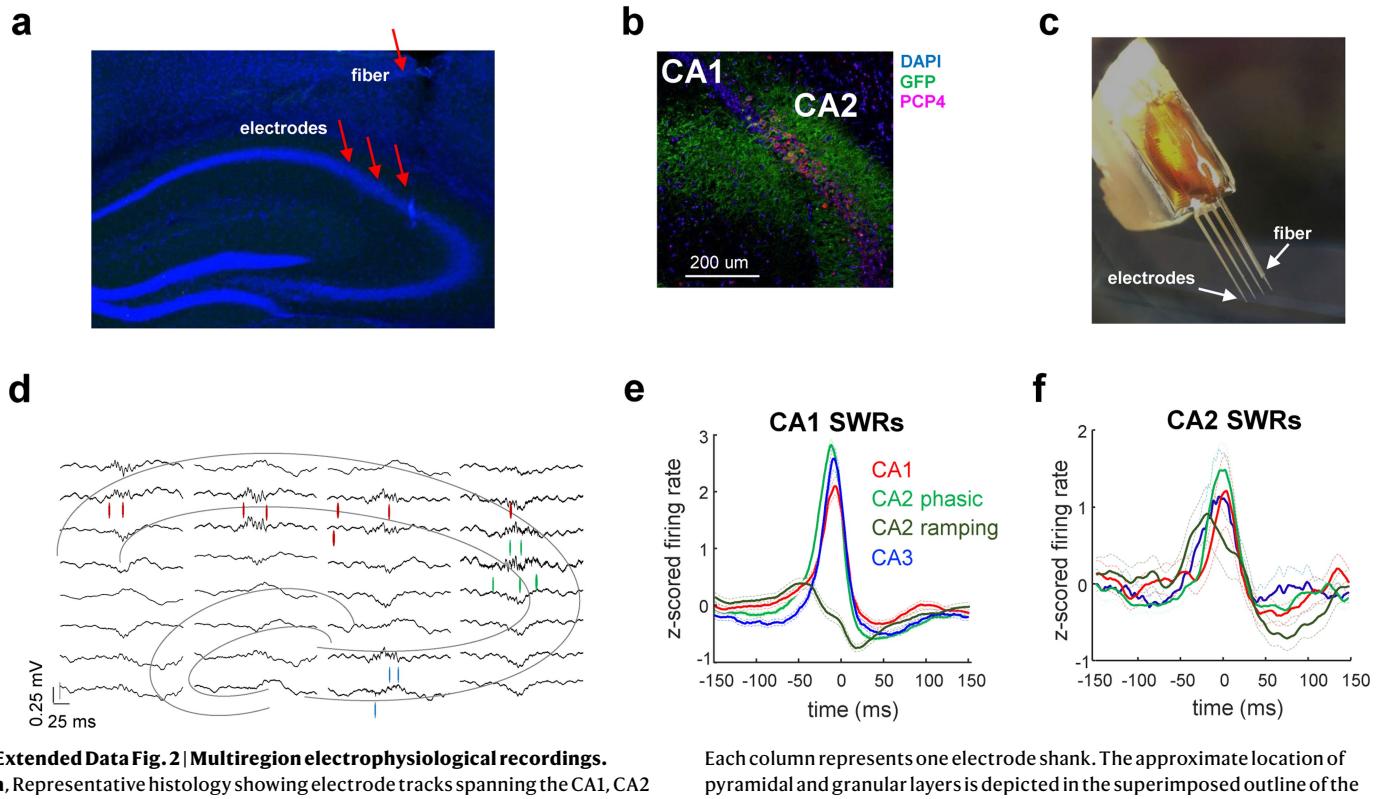
Reprints and permissions information is available at <http://www.nature.com/reprints>.



Extended Data Fig. 1 | Behavioural features during a social-memory task. **a**, Representative animal trajectories during the task show greater time spent around the novel animal (red) in the test (recall) trial. **b**, Example video frame showing pose estimation calculated with DeepLabCut (colour markers). Interaction zones were defined as 10 cm by 10 cm squares (dotted lines) in the two corners in which the cups were located. **c**, The average speed of the animals was not different among trials ($F(2) = 0.92, P > 0.05$; one-way ANOVA). **d**, The average speed inside interaction zones around S_1 (left plot), S_2 or a novel mouse (middle plot) did not differ among trials ($F(2) = 3.14, P > 0.05$; one-way ANOVA). The average speed did not differ outside interaction zones ($F(2) = 1.58, P > 0.05$; one-way ANOVA).

one-way ANOVA). **e**, The left plot shows the total time spent inside the interaction zone around S_1 , S_2 or a novel mouse. The total time spent interacting with a novel mouse during the recall trial was greater than with either familiar mouse in any other trial ($P < 0.01$ for novel versus S_1 interaction during third trial and $P < 0.05$ for novel versus S_1 interaction during all of the other trials; two-way ANOVA mouse \times trial followed by Tukey's post hoc test for multiple comparisons). The right plot shows that the total time spent outside interaction zones was not different between trials ($F(2) = 0.58, P > 0.05$; one-way ANOVA). ** $P < 0.01$, * $P < 0.05$, rank-sum test; n.s., not significant.

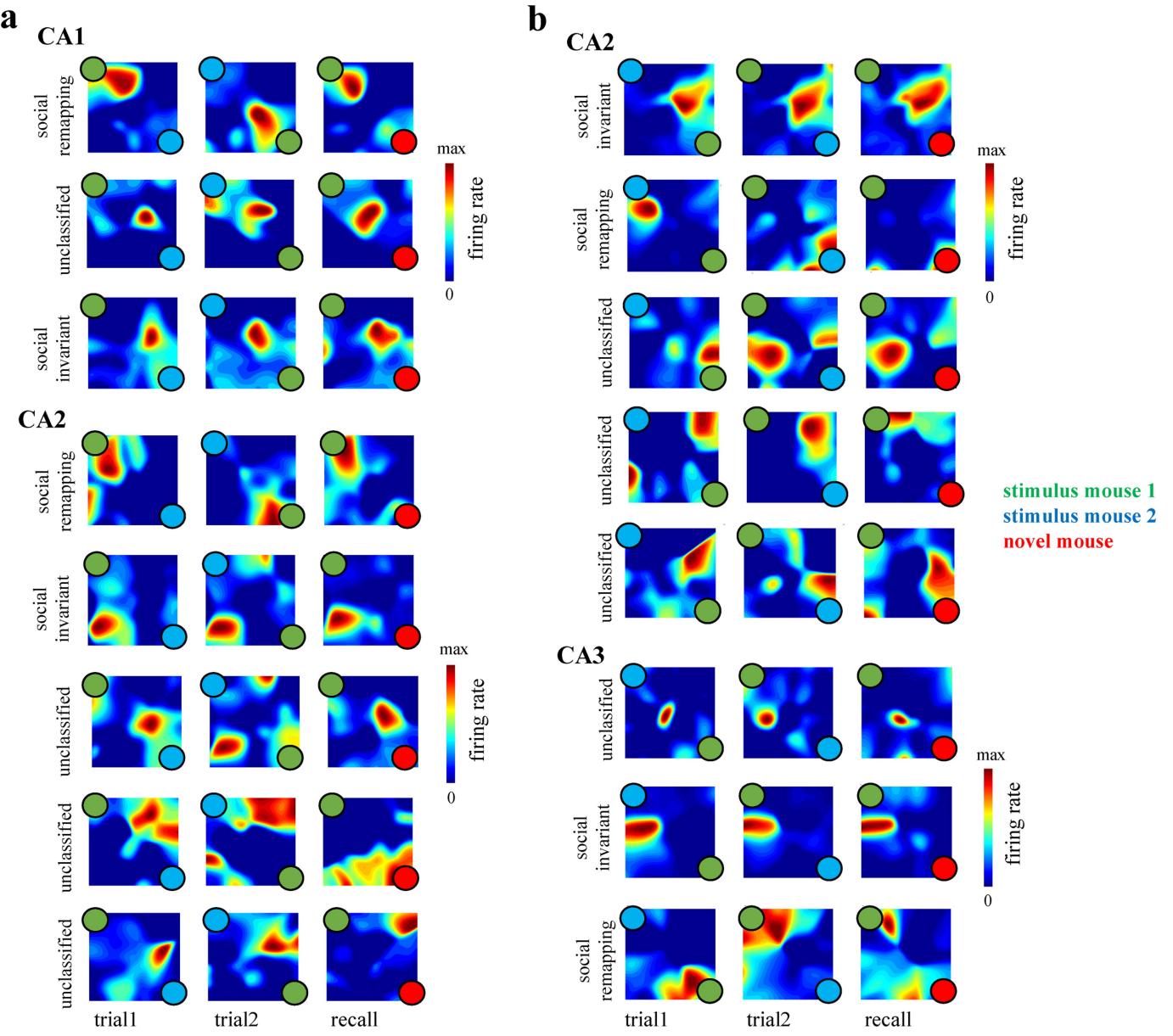
Article



Extended Data Fig. 2 | Multiregion electrophysiological recordings.

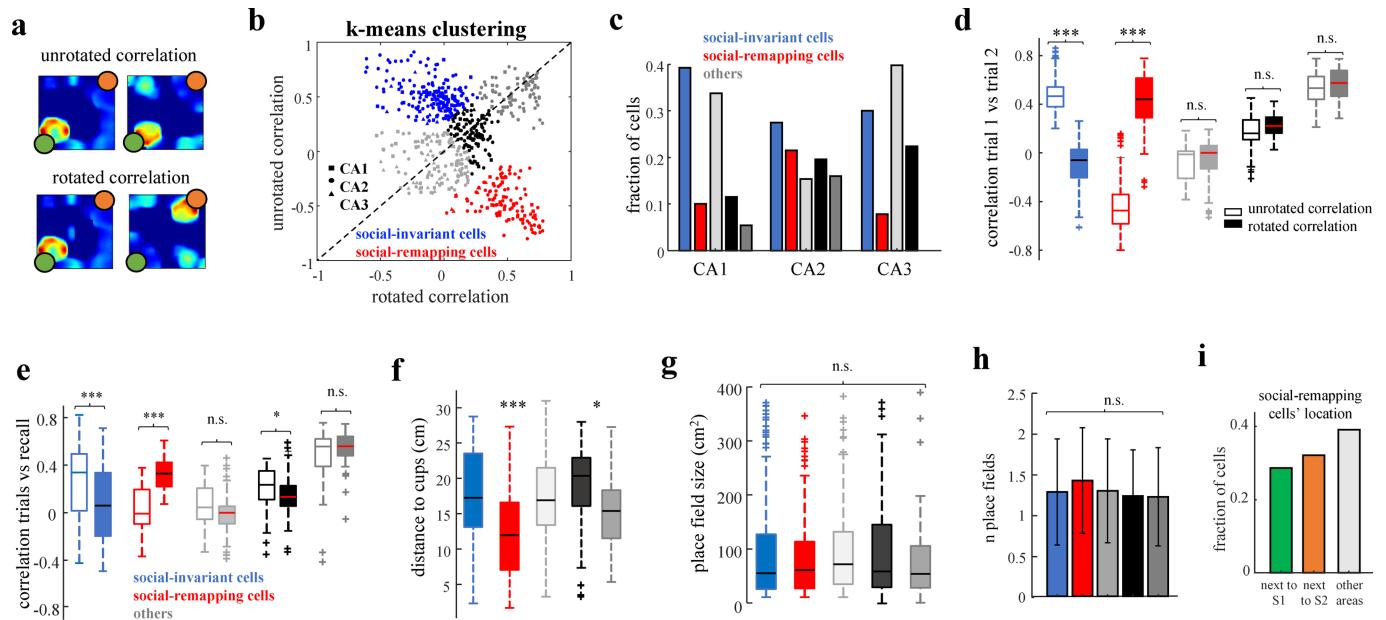
a, Representative histology showing electrode tracks spanning the CA1, CA2 and CA3 areas, with optical fibre over the CA2 pyramidal layer. Blue, DAPI staining. **b**, ChR2-GFP expression in CA2. Blue, DAPI; green, GFP; pink, PCP4. **c**, Silicon probe with 100- μ m optic fibre glued to one electrode shank, mounted in a movable microdrive to allow for precise localization of the target area. **d**, Representative sample recordings of LFPs (one trace per electrode) and single units (coloured lines show spikes) in several regions of the hippocampus.

Each column represents one electrode shank. The approximate location of pyramidal and granular layers is depicted in the superimposed outline of the hippocampus. **e**, Average firing responses of single cells from different regions aligned to SWRs detected in CA1 ('CA1SPW-Rs'). Note that CA2 cells fired before CA1 and CA3, and that a subpopulation of CA2 units ('CA2 ramping') became silent upon SWR onset. **f**, As in **e**, but with firing responses aligned to ripples detected in CA2. Note that CA2 cells are strongly activated during CA2 ripples. These results replicate a previous study of rats⁹.



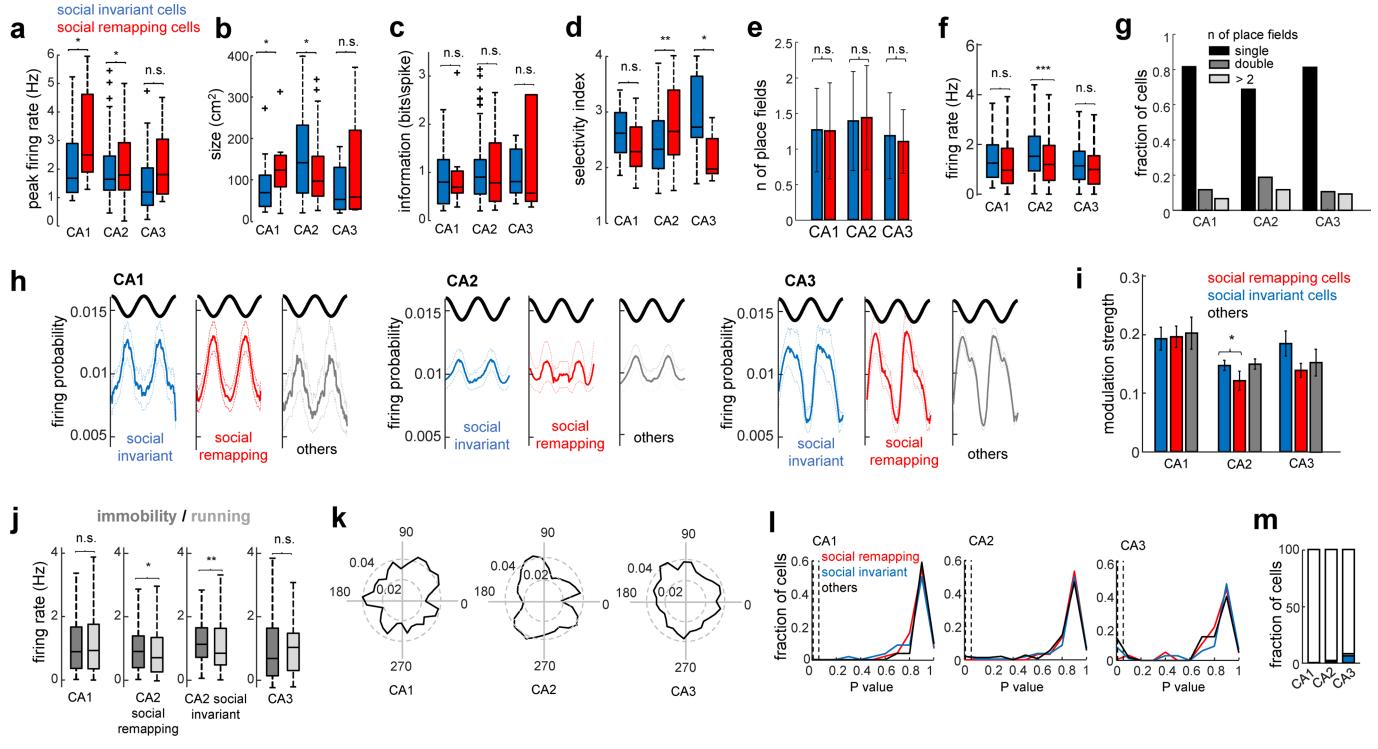
Extended Data Fig. 3 | Classification of single-cell responses during a social-memory task. a, Examples of simultaneously recorded place cells from CA1 and CA2 regions in one mouse. Each row shows the firing map of one cell; firing maps for trial 1, trial 2 and the memory test (recall) session are shown in

each column. Coloured circles represent different stimulus mice. **b,** Another example of simultaneously recorded place cells, from CA2 and CA3 in a second mouse.



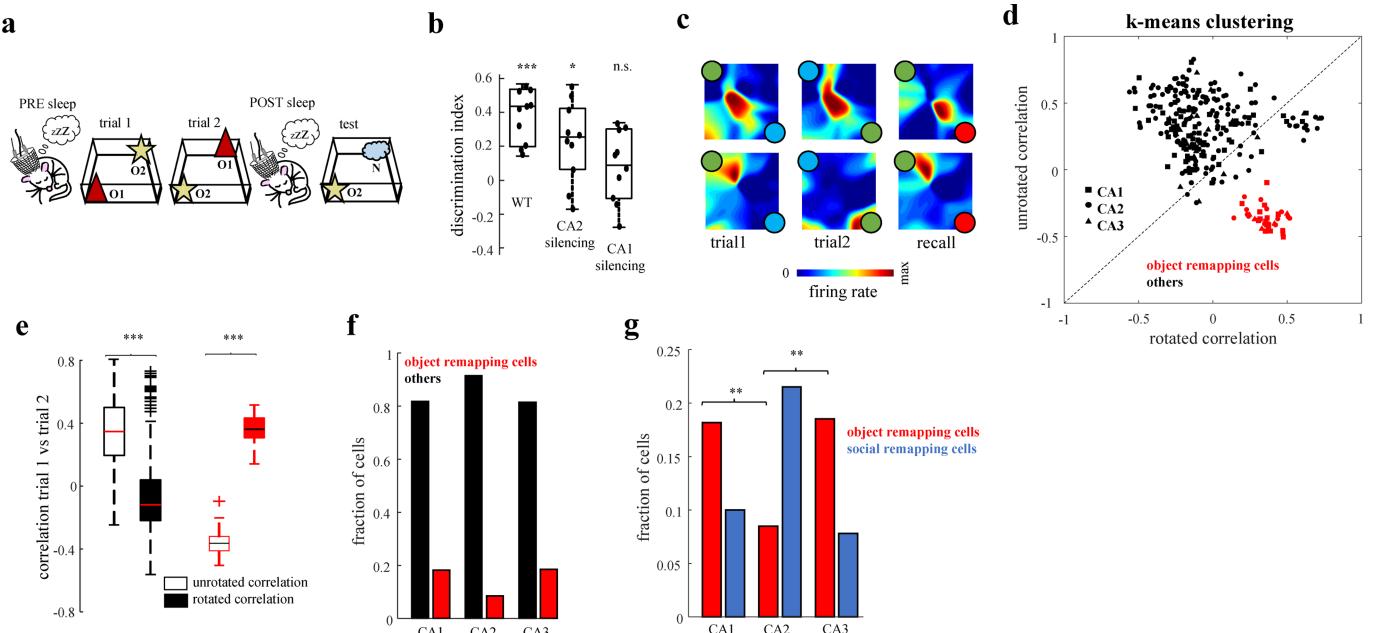
Extended Data Fig. 4 | Classification of single-cell responses during a social-memory task. **a**, Top, the unrotated correlation was computed as the averaged pixel-wise correlation of the firing maps from trials 1 and 2. Bottom, the rotated correlation was calculated after rotating the map for trial 2 by 180°. **b**, K-means clustering of unrotated and rotated spatial correlation values for all cells resulted in five clusters (different colours). One cluster (blue) had high unrotated and negative rotated correlations, and are termed social-invariant cells. Another cluster (red) had high rotated and negative unrotated correlation, and are termed social-remapping cells. The other clusters (light grey, dark grey and black) had more similar values for the two correlations. Squares denote CA1, circles CA2 and triangles CA3 pyramidal cells. **c**, Proportion of CA1, CA2 and CA3 cells from each of the five clusters, colour-coded as in **b**. **d**, Distribution of unrotated (empty) and rotated (filled)

correlation values between trial 1 and trial 2 for cells in all five clusters. *** $P < 0.001$, rank-sum test. **e**, Distribution of unrotated (empty) and rotated (filled) correlation values between the learning trial and recall trial for cells in all five clusters. * $P < 0.05$, *** $P < 0.001$; rank-sum test. Correlation performed between the recall trial and that learning trial in which the position of the familiar mouse was in the opposite location. **f**, Distance from the centre of mass of the place field to the nearest cup for cells in all clusters ($F(4,677) = 27.34$, $P < 4.6 \times 10^{-21}$; one-way ANOVA). Social-remapping cells had place fields closer to the cups ($P < 0.002$; Tukey's post hoc test). **g**, Place field sizes for cells in all clusters were similar ($F(4,677) = 0.39$, $P > 0.05$; one-way ANOVA). **h**, The number of place fields per cell was similar for all clusters ($F(4,677) = 0.68$, $P > 0.05$; one-way ANOVA). **i**, The fraction of social-remapping cells with place fields next to mouse S₁, mouse S₂ and other locations.



Extended Data Fig. 5 | Place-cell properties of social-invariant and social-remapping cells across regions during the social-discrimination task. **a–e**, Place-cell properties for CA1, CA2 and CA3 social-invariant and social-remapping cells. **a**, Peak firing rate; **b**, place field size; **c**, spatial information in bits per spike; **d**, spatial selectivity index; **e**, number of place fields per cell. **f**, Whole-session average firing rate for social-remapping and social-invariant cells from the different subregions. **g**, Fraction of cells with 1, 2 or more place fields in the different regions. **h**, Theta firing phase distribution (firing probability per bin of phases) for social-remapping, social-invariant and other cells from different regions. Rayleigh's test was used against the null

hypothesis (see Methods). **i**, Mean vector length of a cell's firing ('modulation strength') during theta oscillations for CA1, CA2 and CA3 pyramidal cells. **j**, Average firing rate for CA1, CA2 and CA3 cells during immobility and running (at a velocity greater than 5 cm s^{-1}) periods during the task. * $P < 0.05$, ** $P < 0.01$; rank-sum test. **k**, Representative examples of CA1, CA2 and CA3 cell firing rate (shown as distance from origin) as a function of head direction. **l**, Distributions of P -values show a similar lack of head direction tuning for social-remapping, social-invariant and other cells in CA1, CA2 and CA3 regions. Dashed line, $P = 0.05$. **m**, Proportions of social-invariant, social-remapping and other cells that were significantly modulated by head direction ($P < 0.05$) per region.

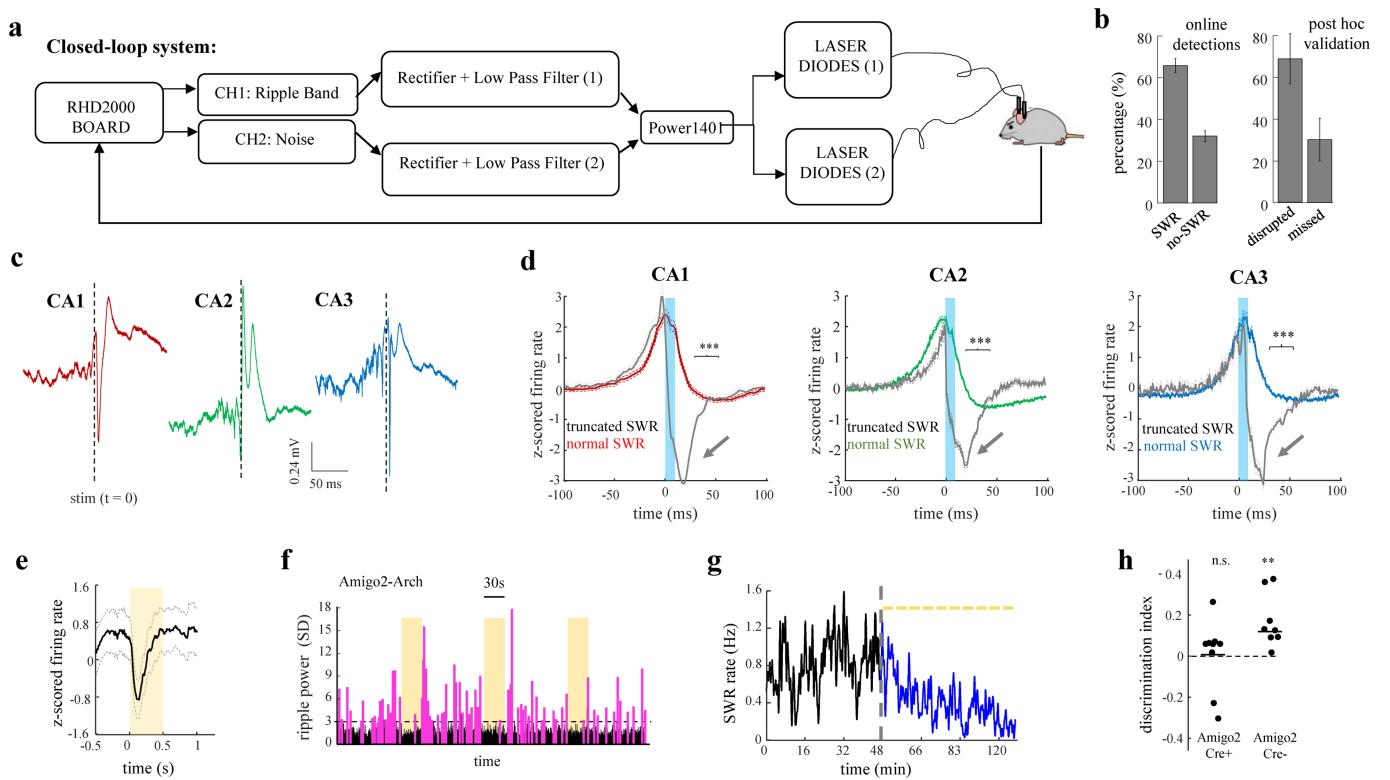


Extended Data Fig. 6 | Object-recognition task: single-cell responses, optogenetic manipulations and reactivation properties per region.

a, Schema of the task. The behavioural paradigm used to assess social memory was also used to assess object-recognition memory. Two previously unseen objects (O1 and O2) were presented for 5 min in the first trial; the position of the objects was then swapped in a second trial of another 5 min. After a home-cage period of 1 h, a memory-recall test trial was performed with one of the previous objects and one novel object (N). **b**, Performance of the discrimination index for animals in the test trial, for wild-type (WT) mice (where the discrimination index was significantly greater than 0; $P < 0.001$, t -test; $n = 10$ sessions with 4 animals), mice with CA2 silenced in trials 1 and 2 during the interaction with the specific object presented again in the recall trial (discrimination index significantly greater than 0; $P < 0.05$, t -test; $n = 10$ sessions in 10 animals), and mice with CA1 silenced in trials 1 and 2 during interaction with the specific

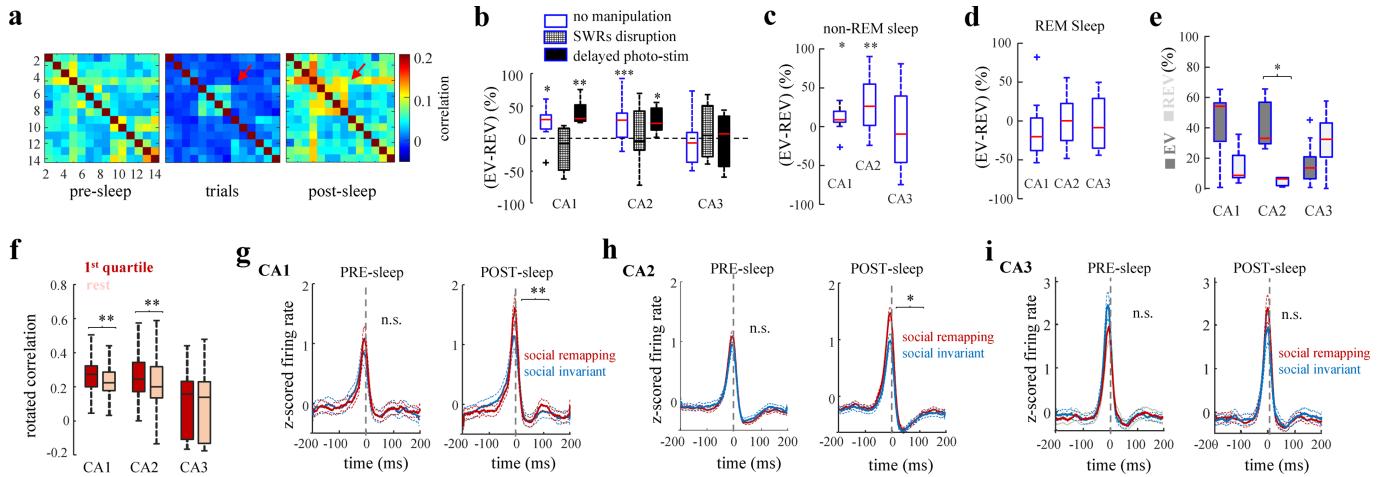
object presented again in the recall trial (discrimination index not significantly different from 0; $P > 0.05$, t -test; $n = 10$ sessions in 10 animals). **c**, Examples of firing maps for two CA2 cells (green and blue) in the object memory task. The first cell had a stable place field in the two learning and test trials, while the second remapped to follow the position of one object. **d**, K-means clustering of unrotated and rotated spatial correlation values for all cells. The red cluster corresponds to a subset of cells ('object-remapping cells') with high rotated and negative unrotated correlation, analogous to social-remapping cells. Squares denote CA1, circles CA2 and triangles CA3 pyramidal cells.

e, Distribution of unrotated (empty) and rotated (filled) correlation values for the two clusters of cells in **d**. *** $P < 0.001$; rank-sum test. **f**, Proportion of CA1, CA2 and CA3 cells from each of the two clusters in **d**. **g**, Proportion of object-remapping and social-remapping cells in CA1, CA2 and CA3. ** $P < 0.01$; Fisher's exact test.



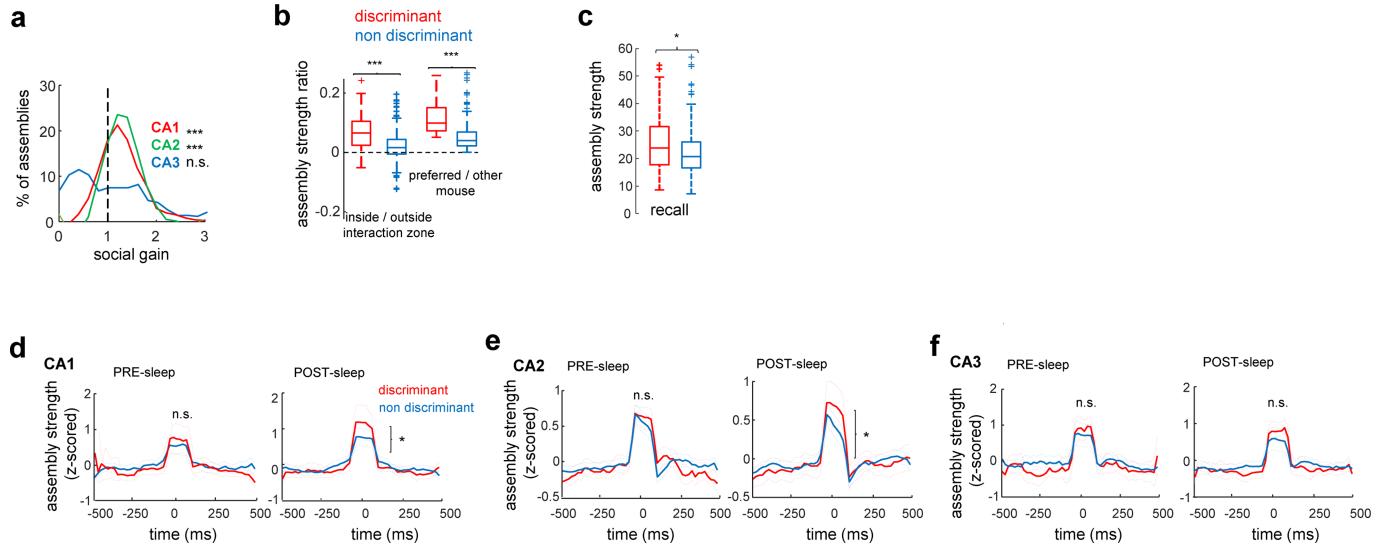
Extended Data Fig. 7 | Effect of optogenetic disruption of SWRs on firing rates and field potentials, and reactivation of hippocampal cells during SWRs. **a**, The closed-loop SWR truncation system: two signals (for real positive events—‘ripple band’—and noise) are extracted from the recording board and filtered in the ripple band (100–300 Hz); a waveform rectifier and a low-pass filter are applied (using a CED 1401 device); upon detection of a positive event (real positive event = 1 and noise = 0), two current sources are triggered and light is delivered bilaterally through the optic fibres connected to the animal. **b**, Estimation of detection performance. Left graph, a subsample of events detected by our on-line system in three sessions ($n=1,000$) was validated by ground truth (offline detected events); the plot shows percentage of true positives (SWR) versus false positives (no-SWR). Right graph, a subsample of true events (detected offline) in three sessions ($n=1,000$) were cross-validated with our online detector to quantify the percentage of events detected (SWRs disrupted) and missed. **c**, CA1, CA2 and CA3 LFP patterns during CA2 SWR disruption. **d**, CA1, CA2 and CA3 average firing responses to normal and truncated SWRs show strong suppression of firing after stimulation with light (blue bar) ($n=53, 148, 87$ CA1, CA2, CA3 cells; $P<10^{-6}, 9.7\times10^{-7}, 1.14\times10^{-8}$, respectively; rank-sign test). **e**, The firing of CA2 pyramidal cells was

suppressed by brief yellow-light pulses (yellow rectangle) in Amigo2-Cre animals expressing AAV2/5 EF1a.DIO.eArch3.0-eYFP in CA2. Curves show mean and s.e.m. ($n=58, P<0.03$; rank-sign test). **f**, Example session in which 30-s pulses of yellow light (yellow bars) were delivered once every two minutes to the CA2 region of Amigo2-Cre mice expressing eArch3.0. The black trace shows ripple-band (100–300 Hz) power in the CA1 pyramidal layer, and magenta traces shows detected SWRs. Note the suppression of CA1 SWRs during illumination. **g**, Example session showing the decreased rate of CA2 SWRs owing to photoactivation of eArch3.0 ($P<0.0246$; Wilcoxon’s rank-sum test). The yellow dashed line shows the period of light stimulation, and the black and blue traces show SWR rate before and during the period of photostimulation, respectively. **h**, Social-memory recall was suppressed following CA2 silencing by yellow-light pulses (30 s, once every 2 min) during the post-sleep period in Amigo2-Cre mice injected with AAV-DIO-eArch3.0 ($n=9$; discrimination index not significantly different from 0; $P>0.05$, t -test), whereas social memory was present in Cre⁺ littermate controls injected with the same virus and receiving the same light pulses ($n=8$; discrimination index differed significantly from 0; $P<0.01$).



Extended Data Fig. 8 | Reactivation of hippocampal cells during SWRs following social learning. **a**, Firing-rate correlation matrices for an example session (all cell pairs) during pre-sleep, learning trials and post-sleep sessions. The colour bar shows colour-coded r values. Note the increase in post-sleep coactivation in some cell pairs that were coactive during the task (red arrow). **b**, (EV – REV) measure of post-sleep reactivation of correlated firing during learning trials in control sessions ('no manipulation'), sessions with optogenetic SWR disruption, and sessions with random optogenetic stimulation. Significant reactivation was observed in CA1 and CA2 control sessions ($P=0.03$ and 0.0028 , respectively; Wilcoxon's rank-sum test) or following random stimulation ($P=0.008$ and 0.04 for CA1 and CA2, respectively, Wilcoxon's rank-sum test). There was no significant reactivation in CA1 or CA2 with SWR disruption. CA3 failed to show significant reactivation

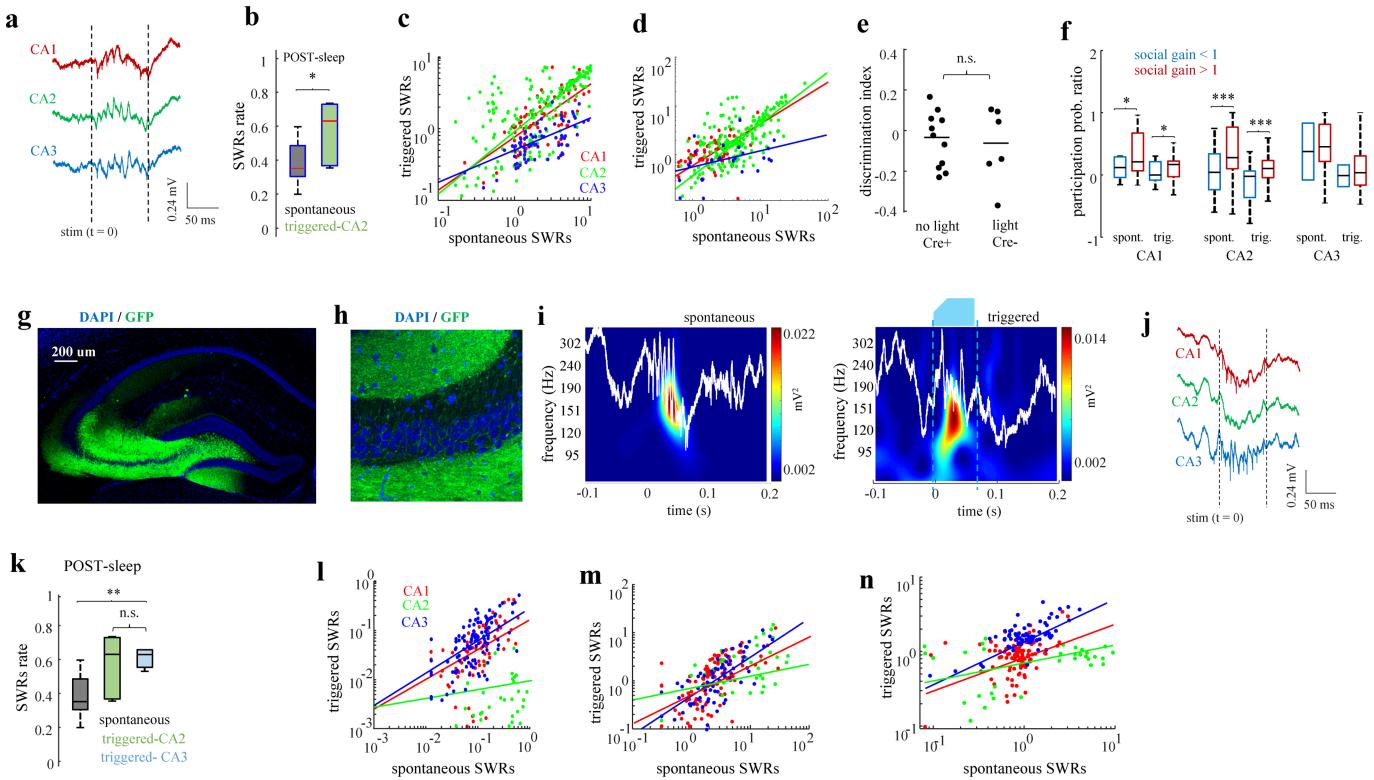
in any session ($P>0.05$). **c, d**, Significant reactivation (EV – REV) was observed in CA1 ($P<0.05$, t -test) and CA2 ($P<0.01$) during the entire slow-wave sleep period (c) but not the REM sleep period ($P>0.05$, t -test) (d). **e**, EV and REV for a subsample of approximately the same number of cells for different regions (CA1, $n=73$; CA2, $n=69$; CA3, $n=67$). **f**, Cells from CA1 and CA2 that contributed the most to the total explained variance (first quartile) had a significantly higher rotated spatial correlation (social-remapping) than the rest of the cells ($P=0.0354$ and $P=0.0223$ for CA1 and CA2 respectively; $P>0.05$ for CA3; Wilcoxon's rank-signed test). **g-i**, Average peri-SWR firing-rate responses for social-remapping and social-invariant cells from CA1 (g), CA2 (h) and CA3 (i) region in pre- and post-sleep. Note that social-remapping cells show higher SWR firing rates in post-sleep but not pre-sleep sessions (CA1, $n=151$, $P=0.0055$; CA2, $n=306$, $P=0.016$; CA3, $n=79$, $P>0.05$).



Extended Data Fig. 9 | Strength of assembly activity during the social-memory discrimination task. **a**, Distribution of assembly social-gain values from different regions. Assembly social gain is defined as the mean assembly strength during exploration within the interaction zone, divided by the mean assembly strength during exploration outside the interaction zone. Social gain was significantly greater than 1 for CA1 ($P < 10^{-6}$; rank-sign and CA2 ($P < 10^{-19}$) but not CA3 ($P > 0.05$). **b**, The left pair of bars shows socially related assembly strength ((assembly strength inside social interaction zone minus strength outside social interaction zone)/(sum of strengths)) for social-discriminант and non-discriminант assemblies ($P < 10^{-3}$; rank-sum test). The right pair of bars

shows that the normalized social-discrimination assembly strength (the difference between assembly strength during interaction with the preferred mouse minus the strength during the interaction with the other mouse, divided by the sum of these two strengths) was greater for discriminant compared with non-discriminант assemblies ($P < 10^{-8}$). **c**, Discriminant assemblies were reactivated during the recall trial significantly more strongly than non-discriminант assemblies ($P = 0.0421$). **d-f**, Average peri-SWR activation of discriminant and non-discriminант assemblies in different hippocampal regions is shown for: **d**, CA1, $n = 116$, $P = 0.0252$; **e**, CA2, $n = 213$, $P = 0.0144$; and **f**, CA3, $n = 59$, $P > 0.05$.

Article



Extended Data Fig. 10 | Generation of CA2 ripple oscillations enhances social-memory recall. **a**, LFPs showing ripple activity in CA1 (red), CA2 (green) and CA3 (blue) in response to optogenetic triggering of ripple in CA2. **b**, Rate of ripples in sessions with optogenetic triggering of SWRs ('artificial CA2') was significantly higher than in control sessions ('spontaneous') ($P < 0.05$, rank-sum test). **c**, Firing rates of all pyramidal cells during spontaneous versus optogenetically triggered CA2 ripples were highly correlated (CA1, $n = 67$, $r = 0.63$, $P < 10^{-13}$; Pearson's correlation; CA2, $n = 147$, $r = 0.75$, $P < 3 \times 10^{-22}$; CA3, $n = 40$, $r = 0.48$, $P = 0.01$). **d**, Firing-rate gain (increase in firing rate during ripples, divided by average firing rate) of pyramidal cells during spontaneous versus triggered ripples for CA1 ($n = 67$, $r = 0.57$, $P < 10^{-6}$), CA2 ($n = 147$, $r = 0.74$, $P < 3 \times 10^{-35}$) and CA3 ($n = 40$, $r = 0.25$, $P > 0.05$). **e**, Social-discrimination indices for Amigo2-Cre⁻ littermate controls injected with Cre-dependent ChR2 AAV with ($n = 6$, $P > 0.05$) and without ($n = 10$, $P > 0.05$) light stimulation did not differ. **f**, Effect of social gain on a neuron's ripple participation gain (post-sleep participation minus pre-sleep participation, divided by their sum). CA1 and CA2 cells showed greater ripple participation gain for cells with positive versus negative social gain for both spontaneous SWRs (CA1 and CA2, $n = 67$ and $n = 147$; $P < 0.05$ and $P < 3.4 \times 10^{-3}$, respectively) and triggered SWRs (CA1 and CA2, $P < 0.05$ and $P < 2.8 \times 10^{-3}$, respectively). CA3 ripple participation gain

showed no effect of social gain for either type of SWR ($n = 40$, $P > 0.05$). **g**, Histology of CA3-implanted Grk-4 animals, previously injected with Cre-dependent AAV expressing ChR2-eYFP (green). **h**, Close-up view of the CA3 area. **i**, Examples of spontaneous and optogenetically triggered ripples in CA3. White lines are LFPs from CA2; colour maps show wavelet spectrograms; dashed lines demarcate the period of illumination. **j**, LFPs showing ripple activity in CA1 and CA3 but not CA2 after optogenetic triggering of ripples in CA3. **k**, The rate of events in sessions with CA3-triggered ripples was significantly higher than in non-stimulated sessions ($P < 0.003$), with no significant difference compared with the rate of ripples in response to CA2-triggered ripples ($P > 0.05$). **l**, The participation probability (the fraction of ripples in which a neuron fires at least one spike) of all pyramidal cells during spontaneous versus triggered CA2 ripples was highly correlated (CA1, $n = 96$, $r = 0.66$, $P < 7 \times 10^{-10}$, Pearson's correlation; CA2, $n = 67$, $r = 0.34$, $P < 3 \times 10^{-22}$; CA3, $n = 112$, $r = 0.67$, $P = 3 \times 10^{-15}$). **m**, A similar result was obtained by comparing firing rates (CA1, $r = 0.59$, $P < 2 \times 10^{-7}$; CA2, $r = 0.49$, $P < 1.7 \times 10^{-5}$; CA3, $r = 0.66$, $P < 8 \times 10^{-10}$). **n**, The firing-rate gain (in-ripple firing rate divided by baseline firing rate) showed similar tendencies (CA1, $r = 0.63$, $P < 1.6 \times 10^{-12}$; CA2, $r = 0.47$, $P < 2.1 \times 10^{-3}$; CA3, $r = 0.71$, $P < 1.7 \times 10^{-18}$).

Reporting Summary

Nature Research wishes to improve the reproducibility of the work that we publish. This form provides structure for consistency and transparency in reporting. For further information on Nature Research policies, see our [Editorial Policies](#) and the [Editorial Policy Checklist](#).

Statistics

For all statistical analyses, confirm that the following items are present in the figure legend, table legend, main text, or Methods section.

n/a Confirmed

- The exact sample size (n) for each experimental group/condition, given as a discrete number and unit of measurement
- A statement on whether measurements were taken from distinct samples or whether the same sample was measured repeatedly
- The statistical test(s) used AND whether they are one- or two-sided
 - Only common tests should be described solely by name; describe more complex techniques in the Methods section.*
- A description of all covariates tested
- A description of any assumptions or corrections, such as tests of normality and adjustment for multiple comparisons
- A full description of the statistical parameters including central tendency (e.g. means) or other basic estimates (e.g. regression coefficient) AND variation (e.g. standard deviation) or associated estimates of uncertainty (e.g. confidence intervals)
- For null hypothesis testing, the test statistic (e.g. F , t , r) with confidence intervals, effect sizes, degrees of freedom and P value noted
 - Give P values as exact values whenever suitable.*
- For Bayesian analysis, information on the choice of priors and Markov chain Monte Carlo settings
- For hierarchical and complex designs, identification of the appropriate level for tests and full reporting of outcomes
- Estimates of effect sizes (e.g. Cohen's d , Pearson's r), indicating how they were calculated

Our web collection on [statistics for biologists](#) contains articles on many of the points above.

Software and code

Policy information about [availability of computer code](#)

Data collection Electrophysiological recordings were conducted using Intan RHD2000 interface board sampled at 20 kHz.

Data analysis Data analysis was performed with custom Matlab scripts that can be downloaded from <https://github.com/buzskilab/buzcode> and <http://fmatoolbox.sourceforge.net/>. Spike sorting was performed semi-automatically, using 'Kilosort' (<https://github.com/cortex-lab/KiloSort>), followed by manual adjustment of the waveform clusters using the software 'Phy' (<https://github.com/kwikteam/phy>).

For manuscripts utilizing custom algorithms or software that are central to the research but not yet described in published literature, software must be made available to editors and reviewers. We strongly encourage code deposition in a community repository (e.g. GitHub). See the Nature Research [guidelines for submitting code & software](#) for further information.

Data

Policy information about [availability of data](#)

All manuscripts must include a [data availability statement](#). This statement should provide the following information, where applicable:

- Accession codes, unique identifiers, or web links for publicly available datasets
- A list of figures that have associated raw data
- A description of any restrictions on data availability

Data and analytical tools used in the paper will be made available upon request.

Field-specific reporting

Please select the one below that is the best fit for your research. If you are not sure, read the appropriate sections before making your selection.

Life sciences

Behavioural & social sciences Ecological, evolutionary & environmental sciences

For a reference copy of the document with all sections, see nature.com/documents/nr-reporting-summary-flat.pdf

Life sciences study design

All studies must disclose on these points even when the disclosure is negative.

Sample size	No specific analysis to estimate minimal population sample or group size was used, but the number of animals, sessions, recorded cells and SPW-R events were larger or similar to those employed in previous related works.
Data exclusions	5 were excluded from optogenetic experiments (stated in the methods section) due to insufficient viral expression. Inclusion criteria for cells (cell type, region, firing rate, etc) or sessions (type of behavior, stimulation protocol, etc.) is specified for each analysis through the text.
Replication	Behavioral results were replicated in 5 independent mice cohorts (Amigo2Cre+ ChR2, Amigo2Cre- ChR2, Grik42Cre+ ChR2, Amigo2Cre+ Arch3, Amigo2Cre- Arch3). Electrophysiological manipulation experiments were replicated in multiple animals and behavioral sessions.
Randomization	Allocation of animals to experimental groups and stimulation protocol were randomly assigned.
Blinding	Due to experimental design constraints, the experimenter was not blind to the manipulation performed during the experiment (i.e., optogenetic manipulation).

Reporting for specific materials, systems and methods

We require information from authors about some types of materials, experimental systems and methods used in many studies. Here, indicate whether each material, system or method listed is relevant to your study. If you are not sure if a list item applies to your research, read the appropriate section before selecting a response.

Materials & experimental systems

n/a	Involved in the study
<input type="checkbox"/>	<input checked="" type="checkbox"/> Antibodies
<input checked="" type="checkbox"/>	<input type="checkbox"/> Eukaryotic cell lines
<input checked="" type="checkbox"/>	<input type="checkbox"/> Palaeontology and archaeology
<input type="checkbox"/>	<input checked="" type="checkbox"/> Animals and other organisms
<input checked="" type="checkbox"/>	<input type="checkbox"/> Human research participants
<input checked="" type="checkbox"/>	<input type="checkbox"/> Clinical data
<input type="checkbox"/>	<input type="checkbox"/> Dual use research of concern

Methods

n/a	Involved in the study
<input checked="" type="checkbox"/>	<input type="checkbox"/> ChIP-seq
<input checked="" type="checkbox"/>	<input type="checkbox"/> Flow cytometry
<input checked="" type="checkbox"/>	<input type="checkbox"/> MRI-based neuroimaging

Antibodies

Antibodies used

- rabbit anti-PCP4 (1:200, Sigma-Aldrich, 409 Cat# HPA005792, RRID: AB_1855086)
- chicken anti-GFP (1:1,000, 408 AVES Labs, Cat# GFP-1020, RRID: AB_10000240)

Validation

- Anti-PCP4 (Statement from Sigma Aldrich): "The antibody is developed and validated by the Human Protein Atlas (HPA) project (www.proteinatlas.org). Each antibody is tested by immunohistochemistry against hundreds of normal and disease tissues. The antibodies are also tested using immunofluorescence and western blotting. To view these protocols and other useful information about Prestige Antibodies and the HPA, visit sigma.com/prestige." More information can be found in: <https://www.sigmaaldrich.com/technical-documents/articles/biology/antibody-enhanced-validation.html>
- Anti-GFP: Antibodies are validated by immunohistochemistry and western blots. References of previous validation are: PMID:16958092, PMID:18386786, PMID:19003791, PMID:19003874, PMID:19711380, PMID:19827160, PMID:19882715, PMID:19950390. More can be found in https://antibodyregistry.org/search.php?q=AB_10000240

Animals and other organisms

Policy information about [studies involving animals](#); [ARRIVE guidelines](#) recommended for reporting animal research

Laboratory animals

Adult male C57 mice, 28-32 g, ~3 months old, were used.

Wild animals

NA

Field-collected samples

NA

Ethics oversight

All experiments were approved by the Institutional Animal Care and Use Committee at Columbia University (Zuckerman Institute).

Note that full information on the approval of the study protocol must also be provided in the manuscript.

Dual use research of concern

Policy information about [dual use research of concern](#)

Hazards

Could the accidental, deliberate or reckless misuse of agents or technologies generated in the work, or the application of information presented in the manuscript, pose a threat to:

- | | |
|-------------------------------------|---|
| No | Yes |
| <input checked="" type="checkbox"/> | <input type="checkbox"/> Public health |
| <input checked="" type="checkbox"/> | <input type="checkbox"/> National security |
| <input checked="" type="checkbox"/> | <input type="checkbox"/> Crops and/or livestock |
| <input checked="" type="checkbox"/> | <input type="checkbox"/> Ecosystems |
| <input checked="" type="checkbox"/> | <input type="checkbox"/> Any other significant area |

Experiments of concern

Does the work involve any of these experiments of concern:

- | | |
|-------------------------------------|--|
| No | Yes |
| <input checked="" type="checkbox"/> | <input type="checkbox"/> Demonstrate how to render a vaccine ineffective |
| <input checked="" type="checkbox"/> | <input type="checkbox"/> Confer resistance to therapeutically useful antibiotics or antiviral agents |
| <input checked="" type="checkbox"/> | <input type="checkbox"/> Enhance the virulence of a pathogen or render a nonpathogen virulent |
| <input checked="" type="checkbox"/> | <input type="checkbox"/> Increase transmissibility of a pathogen |
| <input checked="" type="checkbox"/> | <input type="checkbox"/> Alter the host range of a pathogen |
| <input checked="" type="checkbox"/> | <input type="checkbox"/> Enable evasion of diagnostic/detection modalities |
| <input checked="" type="checkbox"/> | <input type="checkbox"/> Enable the weaponization of a biological agent or toxin |
| <input checked="" type="checkbox"/> | <input type="checkbox"/> Any other potentially harmful combination of experiments and agents |